BBA - Molecular Basis of Disease 1870 (2024) 166993

Contents lists available at ScienceDirect

BBA - Molecular Basis of Disease

journal homepage: www.elsevier.com/locate/bbadis

Cholesterol redistribution triggered by CYP46A1 gene therapy improves major hallmarks of Niemann-Pick type C disease but is not sufficient to halt neurodegeneration

Maria João Nunes [a,b], Andreia Neves Carvalho [a,b], Joana Reis [a], Daniela Costa [a,1], Miguel Moutinho [a,2], Joana Mateus [c,d], Rita Mendes de Almeida [a], Sara Brito [a], Daniela Risso [a], Sofia Nunes [a], Margarida Castro-Caldas [a,e], Maria João Gama [a,b], Cecília M.P. Rodrigues [a,b], Sara Xapelli [c,d], Maria José Diógenes [c,d], Nathalie Cartier [f,3], Farah Chali [f], Françoise Piguet [f], Elsa Rodrigues [a,b,*]

[a] Research Institute for Medicines (iMed.ULisboa), Faculty of Pharmacy, Universidade de Lisboa, Lisbon, Portugal
[b] Department of Pharmaceutical Sciences and Medicines, Faculty of Pharmacy, Universidade de Lisboa, Lisbon, Portugal
[c] Instituto de Farmacologia e Neurociências, Faculdade de Medicina, Universidade de Lisboa, Lisbon, Portugal
[d] Instituto de Medicina Molecular João Lobo Antunes, Faculdade de Medicina, Universidade de Lisboa, Lisbon, Portugal
[e] Department of Life Sciences, Faculty of Science and Technology, Universidade NOVA de Lisboa, Caparica, Portugal
[f] NeuroGenCell, INSERM U1127, Paris Brain Institute (ICM), Sorbonne University, CNRS, APHP, University Hospital Pitié Salpètrière, Paris, France

ARTICLE INFO

Keywords:
Niemann-Pick type C disorders
CYP46A1
Brain cholesterol metabolism
Neurodegeneration
Gene therapy

ABSTRACT

Cholesterol 24-hydroxylase (CYP46A1) is an exclusively neuronal cytochrome P450 enzyme responsible for converting cholesterol into 24S-hydroxycholesterol, which serves as the primary pathway for eliminating cholesterol in the brain. We and others have shown that increased activity of CYP46A1 leads to reduced levels of cholesterol and has a positive effect on cognition. Therefore, we hypothesized that CYP46A1 could be a potential therapeutic target in Niemann-Pick type C (NPC) disease, a rare and fatal neurodegenerative disorder, characterized by cholesterol accumulation in endolysosomal compartments. Herein, we show that CYP46A1 ectopic expression, in cellular models of NPC and in Npc1$^{tm(I1061T)}$ mice by adeno-associated virus-mediated gene therapy improved NPC disease phenotype. Amelioration in functional, biochemical, molecular and neuropathological hallmarks of NPC disease were characterized. *In vivo*, CYP46A1 expression partially prevented weight loss and hepatomegaly, corrected the expression levels of genes involved in cholesterol homeostasis, and promoted a redistribution of brain cholesterol accumulated in late endosomes/lysosomes. Moreover, concomitant with the amelioration of cholesterol metabolism dysregulation, CYP46A1 attenuated microgliosis and lysosomal dysfunction in mouse cerebellum, favoring a pro-resolving phenotype. *In vivo* CYP46A1 ectopic expression improves important features of NPC disease and may represent a valid therapeutic approach to be used concomitantly with other drugs. However, promoting cholesterol redistribution does not appear to be enough to prevent Purkinje neuronal death in the cerebellum. This indicates that cholesterol buildup in neurons might not be the main cause of neurodegeneration in this human lipidosis.

1. Introduction

Niemann-Pick type C (NPC) disease is classified as a lysosomal storage disorder caused by mutations in either the NPC1 or NPC2 genes. Approximately 95 % of NPC cases are attributed to mutations in NPC1, with the remaining 5 % being caused by pathogenic variants or defects in NPC2 [1]. *NPC1* is responsible for encoding a polytopic, extensively

* Corresponding author at: Faculty of Pharmacy, Universidade de Lisboa, Av. Prof. Gama Pinto, 1649-003 Lisbon, Portugal.
E-mail address: Elsa.Rodrigues@ff.ulisboa.pt (E. Rodrigues).
[1] Present address: Division of Infection and Immunity, School of Medicine, Cardiff University, Cardiff, UK.
[2] Present address: Department of Anatomy, Cell Biology and Physiology, Indiana University School of Medicine, Indianapolis, IN, 46202, USA.
[3] Present address: AskBio, 47 Boulevard de l'Hôpital, 75,013 Paris, France.

https://doi.org/10.1016/j.bbadis.2023.166993
Received 21 July 2023; Received in revised form 13 December 2023; Accepted 14 December 2023
Available online 22 December 2023

Abbreviations

CYP46A1	Cholesterol 24-hydroxylase
ER	Endoplasmic reticulum
HPβCD	2-Hydroxypropyl-β-cyclodextrin
LE/L	Late endosome/Lysosome
NPC	Niemann-Pick type C

glycosylated transmembrane protein, which is primarily found on the limiting membrane of the late endosome/lysosome (LE/L) [2,3], and *NPC2* for a soluble lysosomal protein. Together, these proteins play a crucial role in facilitating the movement and recycling of cholesterol derived from lipoproteins, guiding it from the LE/L to various cell compartments, such as the endoplasmic reticulum (ER) or plasma membrane. Therefore, decreased function of these proteins leads to endolysosomal dysfunction due to the accumulation of unesterified cholesterol and other lipids, such as glycosphingolipids, sphingomyelin, and sphingosine, which causes the impairment of mobilization and re-esterification of low density lipoprotein (LDL) cholesterol, giving rise to the accumulation of unesterified cholesterol (or free cholesterol) in LE/L due to impaired egress [4].

Although NPC is a neurovisceral disease, in most cases, the dominant feature is the gradual neurodegeneration, including neuronal loss, which leads to progressive motor impairment, reduced weight gain, cognitive decline, and premature death [1,4,5]. Purkinje neurons in the cerebellum are especially sensitive [6–8], although other areas of the brain are also affected such as the cortex, thalamus and brainstem. The molecular mechanism responsible for neuronal death in NPC is still not fully understood. A robust body of evidence suggests that cholesterol sequestration is the primary offending mechanism in NPC [9], which is in line with the observation that early accumulation of cholesterol in neurons precedes neurodegeneration and neuronal loss in NPC1$^{-/-}$ mice [10]. Thus, the dysregulation of brain cholesterol homeostasis in NPC, might underline, to some extent, the neurodegeneration observed in this disease [5]. It has been proposed that deregulated phagocytosis [11], and necroptosis of Purkinje cells, which in turn promotes and amplifies neuroinflammation [12], and microglia activation, are involved in neurodegeneration. Furthermore, the buildup of other lipids, especially sphingosine, can disrupt calcium homeostasis and impact lysosomal trafficking, ultimately resulting in autophagy defects, which are additional characteristics of NPC disorder [13]. In addition, the accumulation of lipids within lysosomes and mitochondrial membranes could trigger oxidative stress, representing another potential pathological mechanism in NPC [14].

Current treatment options for NPC disease are limited. To date, there are no Food and Drug Administration-approved therapies, however, Miglustat (Zavesca®), an imino sugar known for inhibiting glycosphingolipid synthesis and slowing down the neurological deterioration in NPC animal models and human patients, has received approval from the European Medicines Agency [15]. In 2021 fifteen clinical trials were conducted worldwide on the treatment of NPC, ten of which in Phase I - III and related to the administration of 2-Hydroxypropyl-β-cyclodextrin (HPβCD), under the name VTS-270, which has been given Breakthrough Status by the FDA [15]. HPβCD is a cyclic oligosaccharide characterized by a hydrophobic interior. Once absorbed into the LE/L, it facilitates the transportation of unesterified cholesterol to the cytosol, effectively reducing cholesterol accumulation independently of NPC1 and NPC2 proteins. Regardless, therapeutic approaches are still limited, reinforcing a critical need for the progress of knowledge regarding this pathology.

The neuronal-specific cytochrome P450 cholesterol 24-hydroxylase (CYP46A1) is responsible for the conversion of cholesterol into 24S-hydroxycholesterol (24OHC), which accounts for the major elimination pathway of brain cholesterol [16–18]. Not only does this enzyme directly metabolize cholesterol, but it also modulates cholesterol synthesis, and for this reason, it regulates cholesterol turnover in the brain [18,19]. Interestingly, by controlling cholesterol turnover in neurons, CYP46A1 expression levels have a significant impact in memory and learning [19–21]. Our findings suggest that the modulation of cognitive function *in vivo* by CYP46A1 activity is likely linked to changes in protein prenylation. Specifically, ectopic CYP46A1 expression leads to increased prenylation and activation of proteins belonging to the Rho and Rab families [22]. Consequently, CYP46A1 triggers enhanced neuronal dendritic outgrowth and dendritic protrusion density, and in both *in vitro* and *in vivo* settings, it results in elevated synaptic proteins in crude synaptosomal fractions. These effects are attributed to increased tropomyosin-related kinase receptor phosphorylation and its interaction with geranyl transferase I in a cholesterol-dependent manner [23].

Since it has been demonstrated that modulation of CYP46A1 controls neuronal cholesterol homeostasis and synaptic activity, this enzyme has been considered an appealing drug target for the treatment of neurodegenerative disorders. Indeed, using a adeno-associated virus-mediated gene delivery approach *in vivo*, we have shown in mouse models of Alzheimer's Disease [24,25], Huntington's Disease [26], and Spinocerebellar ataxia [27] that CYP46A1 expression strongly improves the clinical, biochemical, and neuropathological phenotypes. All these data had been obtained with direct intraparenchymal delivery to target a specific region of the brain, as in NPC disease is affecting diffusely the cerebellum, we decided to use a new AAV serotype: AAVPHP.eB, that is known to cross the blood brain barrier and have an effective CNS transduction, after intravenous delivery [28,29].

Therefore, herein we aimed to determine if CYP46A1 overexpression *in vivo* by delivering AAVPHP.eB-CYP46A1 to the brain and notably the cerebellum of Npc1$^{tm(I1061T)}$ mice can decrease neurotoxicity and improve disease phenotype. Molecular and neuropathological hallmarks of NPC disease were characterized as well as motor function.

2. Materials and methods

2.1. Animals and treatment

All animal experiments were performed according to the 2010/63/EU Directive and National law (Decreto-Lei n.° 113/2013). The animal facility and the people involved in animal experiments are certified by the Portuguese regulatory entity, Direção Geral de Alimentação e Veterinária (DGAV). All the protocols executed were submitted to the Animal Welfare Committee of IMM animal ethics committee and to DGAV (License nr 002476/2021). All animal experiments were designed and conducted with commitment to the 3Rs.

The NPC mouse model used in this work was developed by Praggastis and colleagues and presents the knock-in of the NPC1^{I1061T} mutation, the most prevalent human mutation that encodes a misfolded protein [30]. The Npc1$^{tm(I1061T)}$ mouse model closely represents the progression of NPC disease in humans, with decreased motor coordination, brain lesions, particularly in the cerebellar area leading to Purkinje cell death, dendritic and axonal abnormalities, lipid storage, and premature death [30].

Homozygous mutants (Npc1$^{tm(I1061T)}$) and wild-type littermates (Npc1$^{+/+}$) were generated by crossing heterozygous mutant males and females, in-house (https://www.jax.org/strain/027704). Mice were housed on a 12 h light-dark cycle with free access to a standard diet and water *ad libitum*, under standardized conditions. Animals were monitored weekly by the experimenters, and more closely by the experienced staff of the animal facility. A total of 44 animals were used (16 Npc1$^{+/+}$ and 28 Npc1$^{tm(I1061T)}$) and the experimental groups were balanced between male and female mice.

After being anesthetized by isoflurane inhalation, a group of wild-type mice received a retro-orbital injection with a dose of 5×10^{11} vg (viral genomes) of adeno-associated viral (AAV) vector AAVPHP.eB-GFP

(WT-GFP, control group, $n = 16$, 9 males and 7 females), while Npc1$^{tm(I1061T)}$ mice received either the same dose of AAVPHP.eB-GFP (NPC-GFP, $n = 15$, 6 males and 9 females) or AAVPHP.eB-HA.CYP (NPC-CYP, $n = 13$, 6 males and 7 females). The AAV vectors were produced by the Vectors Production Center (CPV), within the INSERM UMR1089 research unit (Nantes, France). Mice were injected at 5 weeks of age and their weight was tracked weekly from 5 weeks of age, and throughout the duration of the experience.

Mice were euthanized at week 12 by transcardiac perfusion after deeply anesthetized by isoflurane inhalation. Blood and brain were quickly collected. To minimize the number of animals used, one brain hemisphere was immediately fixed in 4 % paraformaldehyde solution, and then further impregnated in gelatin and frozen to be processed for histology. The other hemisphere was dissected for the isolation of specific brain regions and the tissues were immediately frozen at −80 °C, for future protein, RNA, and DNA isolation. Additionally, the liver was weighed and collected, and other tissues, such as the heart, lung, and intestine were also isolated and stored at −80 °C, for further processing.

2.2. Tissue sample preparation

To obtain homogeneous samples, frozen tissue isolated from the cortex and cerebellum were ground in liquid nitrogen with a mortar and pestle. The collected ground tissues were separated and stored at −80 °C until used for DNA, RNA, or protein isolation.

2.3. Cell culture and transduction with adenovirus encoding human CYP46A1

Primary human fibroblast cultures from skin biopsies from health controls or with clinical and/or morphological diagnosis of Niemann-Pick type C disease, were purchase either at Coriell Institute (healthy control - GM05659; a clinically unaffected mother of monozygotic twins that presents a 1 bp deletion in exon 12 of the NPC1 gene (1920delG) (GM23151); NPC1 patients bearing different mutations such as NPC1$^{I237S/I1061T}$ (GM03123) and NPC1 $^{\mathbf{1920}delG/IVS\mathbf{9\text{-}1009}G>A}$ (GM22870)), or were kindly provided by Doctor Lúcia Lacerda from the Centro Hospitalar Universitário do Porto EPE, Centro de Genética Médica Dr. Jacinto de Magalhães, Portugal (NPC1 $^{I1061T/I1061T}$ and NPC2 patient (NPC2^{G58T})).

The NPC1 $^{I1061T/I1061T}$ fibroblasts were then cultured in low glucose (1 mg glucose/L) Dulbecco Modified Eagles Medium (DMEM) supplemented with 10 % heat inactivated fetal bovine serum (FBS), 2 mM L-glutamine, 250 μg/mL fungizone, 10 mg/ml kanamycin and 100 units/mL penicillin and 100 μg/mL streptomycin (Gibco® by Life Technologies). GM05659 and GM03123 cells were maintained in Eagle's Minimum Essential Medium with Earle's salts (Gibco® by Life Technologies) and supplemented with non-essential amino acids, along with 10 % fetal bovine serum (Corning®) or 15 % FBS in the case of GM23151. DMEM (high glucose) with 2 mM L-glutamine and 10 % fetal bovine serum was used in the GM22870 fibroblasts. All cell lines were cultivated in the presence of 100 units/mL penicillin and 100 μg/mL streptomycin.

Adenovirus encoding GFP (AdGFP) or FLAG-tagged CYP46A1 (AdCYP) were generated by using the pAdTrack/pAdEasy system and previously described [23]. Cultured cells were transduced with each expression vector and after 24 h the media was changed. Cells were maintained for another 72 h.

2.4. Preparation of total protein extracts

Total protein extracts were prepared as previously described [23]. Briefly, the dissociated mouse tissue was homogenized in lysis buffer (50 mM Tris-HCl (pH 7.5), 180 mM NaCl, 1 mM EDTA, and 1 % Triton), supplemented with 1 mM dithiothreitol (DTT), 1 mM sodium orthovanadate, 10 mM sodium fluoride and protease inhibitors cocktail (Roche, Switzerland). Lysates were incubated on ice for 30 min. After sonicating for 4 times, 4 s each cycle, samples were centrifuged at 13,000*g* for 15 min, at 4 °C, and the supernatants were collected and stored at −80 °C. Total protein levels were quantified by the Bradford method, using Bio-Rad Protein Assay Reagent (Bio-Rad Laboratories, Hercules, CA, USA), according to the manufacturer's protocol.

2.5. RNA isolation and reverse transcription

RNA was isolated from the cerebellum and cortex tissue of each mouse using TRIzol reagent (Thermo Fisher Scientific Inc.), according to the manufacturer's instructions. Quantification was performed in the Nanodrop spectrophotometer (Thermo Fisher Scientific Inc.). The RNA samples were stored at −80 °C until further use.

Reverse transcription was performed with the NZY Tech Reverse Transcriptase (NZYTech) after treatment of RNA samples with DNAse I, as previously described [23]. RNA samples were treated with DNAse I Recombinant enzyme (Roche Diagnostics GmbH, Mannheim, Germany). For that, 0,1 U/μL of DNAse I were used to treat 1 μg of total RNA, in 1× incubation buffer. The samples were then heated at 37 °C for 30 min, followed by 10 min at 75 °C, in a VWR Thermal Cycler (VWR International LLC, USA). To synthesize the cDNA, 5 ng/μL of random hexamer mix (NZYTech, Lda., Lisboa, Portugal) and 0.5 mM dNTPs NZYMix (NZYTech, Lda.) were added to the DNAse-treated samples (approximately 500 ng of DNase-treated RNA). After a 5 min incubation at 65 °C, 100 U of NZY Tech Reverse Transcriptase (NZYTech) in reaction buffer 1× was added to the mix. The samples were then incubated at 25 °C for 10 min, followed by 50 min at 50 °C, and 5 min at 85 °C. Until further use, the cDNA samples were stored at −20 °C.

2.6. Reverse transcription quantitative polymerase chain reaction (RT-qPCR)

For detection and quantification of mRNA expression levels in mouse cerebellum and cortex RT-qPCR was run in 384-well optical reaction plates using the SensiFAST™ SYBR® Hi-ROX Kit (Meridian Bioscience Inc., Cincinnati, Ohio, EUA) and 300 nM of specific primers (STAB Vida, Caparica, Portugal) for mice (Supp. Table 1) samples, as previously described [31].

The RT-qPCR was performed in a QuantStudio 7 Flex Real-Time PCR System (Thermo Fisher Scientific Inc.), with the following cycling program: an initial denaturation at 95 °C for 2 min and 40 cycles of 95 °C for 5 s and 60 °C for 30 s, followed by a melting curve analysis. Each sample was run in duplicate and the mRNA levels of the genes of interest were normalized to the mRNA levels of the ribosomal protein large subunit 19 (*Rpl19)* and *Rpl29* genes. Reference genes were selected using the NormFinder software [32]. The normalized levels are presented as fold change from controls using the ΔΔCt method.

2.7. Western blotting and immunodetection

The levels of the proteins of interest were determined by Western blot analysis [31]. Protein samples isolated from brain tissue were denatured for 5 min at 95 °C using a mixture of 1:1 (*v*/v) sample/2× SDS buffer (0.25 mM Tris-HCL (pH 6.8), 4 % SDS, 40 % glycerol, 0.2 % bromophenol blue, 1 % 2β-mercaptoethanol). The denatured proteins were then separated on a 12.5 % or 10 % sodium dodecyl sulfate-polyacrylamide gel electrophoresis (SDS-PAGE). The gel was then electrotransferred to an activated polyvinylidene difluoride (PVDF) membrane (Immobilon®-P, MilliporeSigma, Burlington, Massachusetts, USA). The membranes were then stained with amido black 1× (Sigma-Aldrich, Inc.) and air dried at room temperature. After re-hydration with ethanol, the membranes were incubated with specific primary antibodies (Suppl. Table 2) and with the correspondent secondary antibodies (Suppl. Table 3). Protein detection was performed in a ChemiDoc™ MP imaging system (Bio-Rad Laboratories) using the WesternBright™ ECL (Advansta Corporation, Menlo Park, CA, USA)

Western blotting detection reagent or the SuperSignal™ West Femto Maximum Sensitivity Substrate (Thermo Fisher Scientific Inc.). The relative intensities of protein bands were analyzed using the Image Lab Software Version (Bio-Rad Laboratories).

2.8. Total cholesterol assay

The Amplex® Red Cholesterol Assay Kit (Sigma-Aldrich), was used to evaluate the levels of both free cholesterol and cholesteryl esters in mouse cerebellum and cortex protein extracts, according to the manufacturer's instructions and as previously described [22]. The total protein extracts prepared from cerebellum and cortex mouse samples, as previously described, were diluted 1:50 in 1× reaction buffer and 50 μL of each sample was then placed into a 96-well microplate for fluorescence-based assays in duplicates. In parallel, a cholesterol calibration curve was prepared and applied in the same 96-well microplate. The reaction was initiated by the addition of 50 μL of the reaction mixture containing 300 μM of Amplex® Red reagent, 2 U/mL HRP, 2 U/mL cholesterol oxidase, and 0.2 U/mL cholesterol esterase in 1× reaction buffer. After an incubation of 30 min at 37 °C, the fluorescence was measured in the Varioskan LUX Multimode Microplate Reader (Thermo Fisher Scientific Inc.) with an excitation wavelength of 560 nm and emission detection at 585 nm. Cholesterol levels were normalized to total protein concentration and quantified as μg of cholesterol/mg of protein. Results are presented as fold change to WT-GFP controls.

2.9. Histological processing

The brain hemisphere reserved for immunohistochemistry was immediately fixed in paraformaldehyde 4 % for 48 h. Afterward, the hemispheres were sequentially transferred to a 15 % and 30 % saccharose solution for 48 h each. The tissue was then embedded in gelatin and frozen at −80 °C. Brains were processed in 12 or 20 μm thick sagittal slices using the cryostat. Brain embedding and processing was performed by the Comparative Pathology Unit at Instituto de Medicina Molecular João Lobo Antunes (iMM).

2.10. Immunohistochemistry and filipin staining

2.10.1. Human fibroblasts

Fibroblasts were incubated with 75 nM Lysotracker® Red DND-99 for 1 h at 37 °C humidified atmosphere of 5 % CO_2 prior to fixation with a solution of 4 % paraformaldehyde in phosphate buffered saline (PBS). Subsequently, cells were rinsed with PBS, and incubated with a solution of 50 μg/mL filipin III in PBS for 2 h at room temperature. Cells were then washed with PBS and mounted. Fluorescence visualization was performed in an AxioScope.A1 microscope (Zeiss, Germany) with an AxioCam HRm camera (Zeiss), by analysis of 5 to 10 microscopic fields. Fluorescence and co-localization quantification are presented as average intensity/cell and were performed using Fiji software.

2.10.2. Mouse brain slices

To assess microglia and astrocytes activation, Anti-ionized calcium-Binding Adapter Molecule 1 (IBA-1) and Glial fibrillary acidic protein (GFAP) immunohistochemistry were performed, respectively, in parasagittal cerebellum slices of each mouse. Mouse cerebellum sections were also immunostained for Calbindin and the HA-Tag, for the visualization of Purkinje cells and the ectopically expressed CYP46A1, respectively. For all antibodies, the same procedure was followed. Briefly, slices were air-dried for 1 h and rehydrated in PBS for 10 min, before incubation with blocking solution (goat serum 5 % and Triton X-100 0.2 % in PBS) for 1 h, in a humid chamber protected from light and at room temperature. After blocking, the slices were then probed with either primary antibody (Suppl. Table 4) diluted in blocking solution, overnight, in a humid chamber at 4 °C, and protected from light. Unbound primary antibodies were washed with PBS and the slices were incubated for 1 h at room temperature in a humid chamber and protected from light with the respective secondary antibodies (Suppl. Table 5) and DAPI (1:2000; Biotium) diluted in blocking solution. Slices were washed again with PBS and then mounted in Mowiol® mounting media (Sigma). Fluorescence visualization was performed in an AxioScope.A1 microscope (Zeiss, Germany) with an AxioCam HRm camera (Zeiss). Morphological analysis and fluorescence quantification were performed in 5 to 10 microscopic fields using NIH ImageJ 1.46r software. A blinded acquisition and analysis of Iba-1 fluorescence was performed. To further assess astrocytic morphological features, slices stained for GFAP were also visualized in a Leica TCS SP8 Confocal Microscope (Leica Microsystems, Germany) and analyzed with the Leica Application Suite X software (Leica Microsystems).

For free cholesterol staining, mice brain slices were dyed with filipin III (F4767, Sigma-Aldrich). Briefly, the slices were air-dried and rehydrated in PBS, and, posteriorly, 0.05 mg/mL filipin III was added for 2 h in a humid chamber protected from light and at room temperature. The slices were then washed in PBS and mounted. Fluorescence visualization was performed in an AxioScope.A1 microscope with an AxioCam HRm camera. Blinded analysis of the filipin score of the cortex region of the stained sections was carried out by two independent reviewers, as the sections were previously independently coded by a third party. A scale of 0–6 was used to evaluate filipin staining intensity as an indicator of relative cholesterol storage, being 0 corresponding to no accumulation, and 6 corresponding to extensive storage. After scoring, the third-party code was broken and the results of all sections were averaged for each mouse group (WT-GFP, NPC-GFP, and NPC-CYP).

2.10.3. Purkinje cell count

For the Purkinje cell visualization and count, the 12 μm thick sagittal mouse cerebellum slices were stained with Cresyl Violet. Briefly, the sections were air-dried and stained with filtered Cresyl Violet (Sigma-Aldrich) at 60 °C, for 3 min. Subsequently, the sections were differentiated in 96 % ethanol with acetic acid for 1 min and then dehydrated in a series of ethanol consisting of 96 % ethanol and then 100 % ethanol, for 1 min in each solution. The sections were then clarified in xylene for 1 min. Finally, sections were mounted using Entellan mounting medium (Merck, Rahway, New Jersey, U.S.) and then air-dried. The number of Purkinje cells in each cerebellar lobule (I-X) of the Cresyl Violet-stained sections was manually counted under a 40× objective, using the Invitrogen™ EVOS FL Auto 2 Imaging System. The length of the Purkinje cell layers was manually traced and measured using ImageJ software analysis (National Institutes of Health). The results are presented as the number of Purkinje cells/mm, reflecting the number of cells per length of cell layer for each cerebellar lobe. The staining and quantification of brain slices was blinded, and only afterwards the correspondence to the experimental group was performed.

2.11. Behavioral tests

Behavioral tests were performed from week 6 until week 12. The handling period coincided with the first week after the retroorbital injection at week 5. All animals were handled in cupped hands for a few minutes in four consecutive days so that they became used to the experimenters. Acclimatization of the animals to the testing room and the different apparatus was also performed before the first trial of each test, except for the open field test used to assess individual spontaneous locomotor activity based on the exploratory behavior of mice. All behavioral tests were carried out between 9:00 AM and 6:00 PM and the apparatus used were cleaned with 30 % ethanol between animals' trials. Rotarod and Catwalk tests were performed every 2 weeks while the open field test was performed once, at week 12.

2.11.1. Rotarod test

Mice were tested in a rotarod apparatus specific for mice (Panlab, Harvard Apparatus, Barcelona, Spain) to evaluate their motor

performance, from week 6 to week 12. Retention time was measured in animals subjected to a run of 3 trials, in 2 consecutive days, on a constant 10 rpm rotating drum, for a maximum of 180 s per trial. The latency to fall was registered by the investigator and the best performance is presented for each time point and represents the cumulative retention time of the best run.

2.11.2. Catwalk test

To analyze gait impairment a catwalk test was performed every 2 weeks, from week 6 until week 12. Each animal was placed in a transparent catwalk and its gait in spontaneous locomotion was recorded using a video camera (Webcam Logitech Brio 4 K UHD) placed under the catwalk. Mice moved freely for a maximum of 4 min. Subsequent analysis of the collected recordings was used to determine the stride length for each limb: right and left fore and hindlimbs.

2.11.3. Open field test (OFT)

To assess individual spontaneous locomotor activity, the OFT was utilized. The open field arena was constructed as an empty square wooden box measuring 40 × 40 × 40 cm in height, with virtual divisions into three concentric squares: a peripheral, an intermediate, and a central zone. The testing protocol, previously described in detail [33], involved placing each animal individually in the center of the arena and allowing them to move freely for 5 min. The behavior was recorded *via* video and analyzed using the Smart® tracking software (version 2.5; Panlab, Barcelona, Spain). The center of the animal dorsum was defined as the reference point for tracking its position. Average velocity (cm/s), total travelled distance (cm), number of arena crossings, resting time, and the percentage of time moving slowly or fast were employed to assess locomotor activity. Each animal was tested only once.

2.12. Statistical analysis

For animal experiments, sample size was calculated using the Student's *t*-test, taking into account an expected difference between 25 and 30 % depending on the analyzed outcome, and a coefficient of variation of 15 % (power 90 %, $\alpha = 0.05$). Animals were randomly selected for experimental groups, and littermates were compared for all treatment groups. Outliers were identified using the ROUT method and excluded from the analysis. The Shapiro-Wilk test was performed to test if the data fit a normal distribution. One-way ANOVA, followed by Tukey's multiple comparisons test was used when data fitted a normal distribution. When data failed to pass the normality test, the Kruskal-Wallis test was performed, followed by Dunn's multiple comparisons test. Data analyses and graphical representations were conducted using GraphPad Prism software version 9 (GraphPad Software Inc., San Diego, CA, USA). The results are presented as mean values ± standard error of the mean (SEM), and statistical significance was determined for $p < 0.05$.

3. Results

3.1. CYP46A1 decreases cholesterol accumulation in NPC human fibroblasts

In order to evaluate the potential of CYP46A1 in alleviating the NPC phenotype associated with cholesterol accumulation in the LE/L, human fibroblasts from control, NPC1, and NPC2 individuals were subjected to transduction with an adenovirus carrying GFP (AdControl) or GFP along with FLAG-tagged human CYP46A1 (AdCYP), under control of two separate promoters. The cells were then cultured for 96 h. As controls we used fibroblasts from a healthy donor (GM05659), and from a clinically unaffected mother that presents a 1 bp deletion in exon 12 of the NPC1 gene (1920delG) (GM23151). We also used fibroblasts from NPC1 patients bearing different mutations such as $NPC1^{I1061T/I1061T}$, $NPC1^{237S/I1061T}$ (GM03123), and $NPC1^{1920delG/IVS9\text{-}1009G>A}$ (GM22870), and from a NPC2 patient ($NPC2^{G58T}$). Fibroblasts were incubated with Lysotracker® for LE/L labeling, fixed and stained with Filipin III, to label free cholesterol (Fig. 1). Filipin III, derived from *Streptomyces filipinensis*, is a naturally fluorescent antibiotic that exhibits selective binding to free cholesterol, enabling the detection of cholesterol accumulation patterns. [34].

As expected, the characteristic intracellular accumulation of cholesterol in fibroblast from NPC patients was observed (Fig. 1). Our results also show that ectopic expression of CYP46A1 led to a significant reduction of Filipin III staining by approximately 30 % in $NPC1^{I1061T/I1061T}$ and $NPC2^{G58T}$, and 15 % in $NPC1^{237S/I1061T}$ and $NPC1^{1920delG/IVS9\text{-}1009G>A}$ fibroblasts (Fig. 1B), when compared to the NPC-AdControl condition for each NPC mutation, which reflects a reduction in free cholesterol levels. More importantly, CYP46A1 expression robustly decreased the co-localization between Filipin III and Lysotracker® staining in all the previously mentioned cell lines (Fig. 1C), revealing a reduction in cholesterol entrapment in the LE/L.

These results indicate that CYP46A1 expression leads to a reduction in cholesterol accumulation in the LE/L compartment in human NPC fibroblasts, ameliorating the NPC phenotype.

3.2. CYP46A1 ectopic expression in $Npc1^{tm(I1061T)}$ mice

Our *in vitro* studies in NPC fibroblasts suggest that CYP46A1 ectopic expression leads to an amelioration of the pathological phenotype of intracellular cholesterol accumulation. To determine whether *in vivo* CYP46A1 ectopic expression would be able to improve disease phenotype, CYP46A1 expression was increased in the $Npc1^{tm(I1061T)}$ mouse model [30], through AAV gene-mediated delivery. $Npc1^{tm(I1061T)}$ mice present the knock-in of the $NPC1^{I1061T}$ mutation, the most prevalent human mutation which encodes a misfolded protein. The $Npc1^{tm(I1061T)}$ mouse model faithfully recapitulates human NPC disease, with decreased motor coordination, brain lesions, particularly in the cerebellar area leading to Purkinje cell death, dendritic and axonal abnormalities, lipid storage, and premature death [30].

A group of $Npc1^{tm(I1061T)}$ mice was administered intravenously with a titer of 5×10^{11} vg (viral genomes) of AAVPHP.eB-HA.CYP (NPC-CYP) or AAVPHP.eB-GFP vector (NPC-GFP). In parallel, a group of wild-type mice ($Npc1^{+/+}$) received the AAVPHP.eB-GFP vector (WT-GFP). The systemic delivery of the AAV-PHP.eB serotype efficiently transduces brain cells, particularly across the cortex (layer IV-V) and hippocampus (particularly subregion CA2), and the thalamus, cerebellum, and brainstem [29]. Additionally, depending on the analyzed region, between 85 and 90 % of the transduced cells are neurons [29]. Results presented in Fig. 2 confirm the efficiency of AAV delivery to the cerebellum of WT-GFP (Fig. 2A and D) and NPC-GFP mice (Fig. 2B and E), through the visualization, in parasagittal brain sections, of GFP expression in the Purkinje cells of the cerebellum. The correct delivery of CYP46A1 to the brain in NPC-CYP mice was confirmed by immunofluorescence visualization of the HA-tag (Fig. 2C and F). The confirmation of NPC1 phenotype and of the ectopic expression of CYP46A1 was further performed by Western blot analysis (Fig. 2G), with antibodies against NPC1 and HA-tagged CYP46A1 in mouse cerebellum. CYP46A1 delivery to the cortical region was also confirmed by immunohistochemistry and Western-blot analysis (Suppl. Fig. 1).

Weight loss is one of the hallmarks of the NPC disease and it has already been described for this animal model [30]. Therefore, we tracked mouse weight weekly from the AAV injection onwards (Fig. 3A). WT-GFP animals steadily increased their body weight with time, reaching a body weight gain, when compared to the body weight presented one week after the injection, of approximately 43 % at week 12 for male mice (left panel) and 34 % for females (right panel). NPC-GFP male mice have a maximum increase in weight gain of about 32 % at week 10, while female mice attained a maximum of weight gain of approximately 16 % also at week 10. Interestingly, while NPC-GFP female mice showed a significant decrease in the percentage of weight gain from 10 weeks onwards, this was not the case for NPC-CYP females,

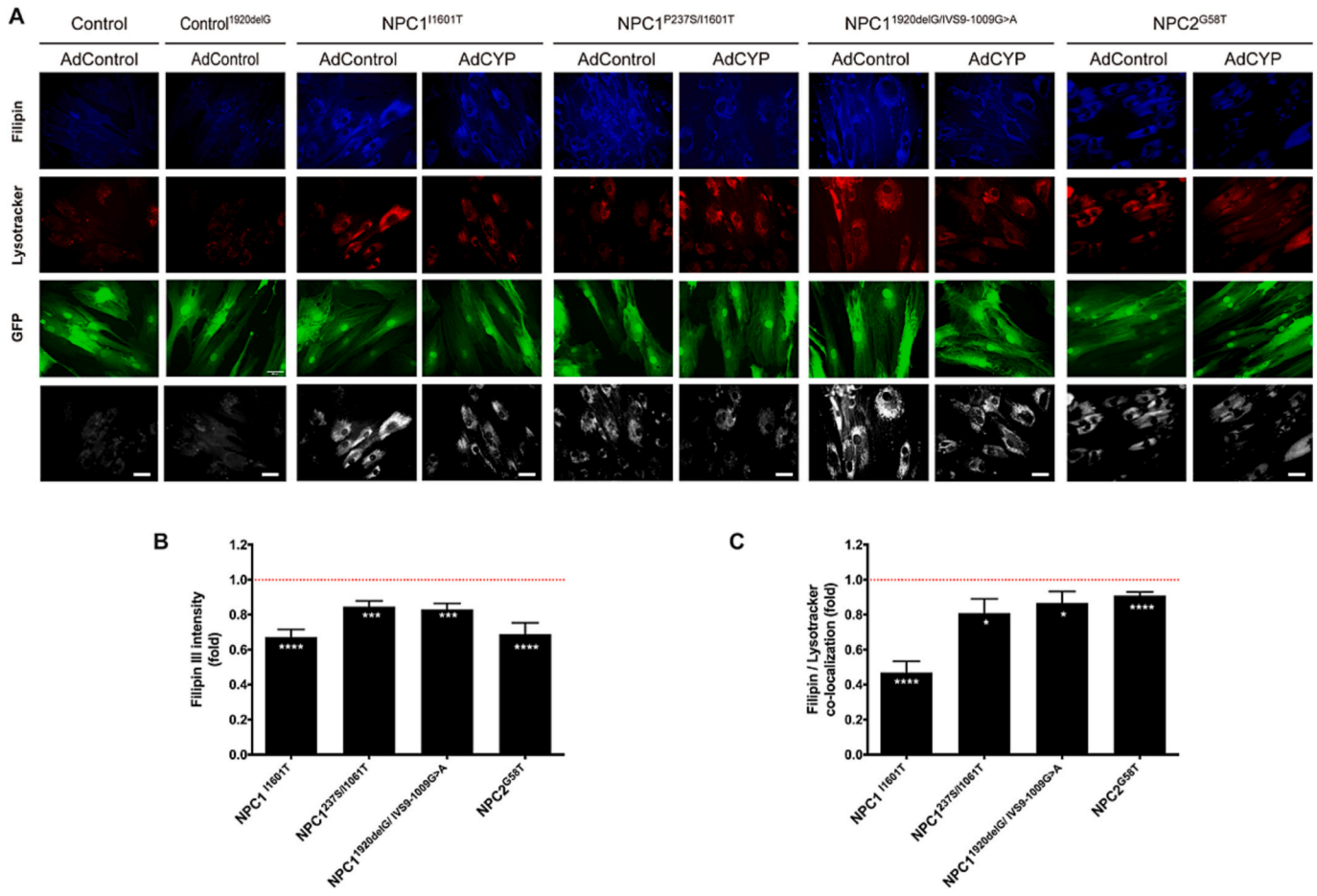

Fig. 1. CYP46A1 reduces cholesterol levels and cholesterol sequestration in the late endosomes/lysosomes compartment in NPC human fibroblasts with different mutations. Fibroblasts from a healthy control (Control), a clinically normal mother of affected monozygotic twins (Control^{1920delG}), NPC1 patients (NPC1$^{I1061T/I1061T}$, NPC1$^{237S/I1061T}$, and NPC1$^{1920delG/\ IVS9\text{-}1009G>A}$, and from a NPC2 patient (NPC2^{G58T}) were transduced with adenovirus encoding GFP (AdControl) or GFP and FLAG-CYP46A1 (AdCYP) and maintained for 96 h. Fibroblasts were incubated with Lysotracker® to stain late endosomes/lysosomes, and subsequently the cells were fixed and stained with Filipin III (free cholesterol staining). Images are representative of Filipin III (blue), Lysotracker® (red) and GFP (green) staining, and co-localized pixels of Lysotracker® and filipin III (white)(scale bar: 20 μm) (A). Filipin III levels were determined by measuring the average fluorescence intensity/cell in each field (B), and the number of co-localized pixels of Lysotracker® and Filipin III/cell was also determined (C). Data represents mean values ± SEM from at least three independent experiments and is expressed as fold change to the NPC- AdControl condition of each cell line. Statistical analysis was performed by Student's *t*-test (*$p < 0.05$, ***$p < 0.001$ and ****$p < 0.0001$ *vs* respective NPC-AdControl).

where a shift in the weight gain curve was only observed at week 12. Indeed, NPC-CYP female mice continued to have a significant positive increment of approximately 21 % in body weight until week 12, while NPC-GFP females started losing weight, as shown by a decrease in gain weight from 15.8 % to 7.6 %, from week 10 to week 12. This difference was not observed in male mice.

In NPC disease, besides the neurological features, liver-associated pathologies are also present in patients [35]. Therefore, the effect of CYP46A1 ectopic expression on liver-to-body weight was evaluated (Fig. 3B). A significant increase of 1.4- fold was observed in NPC-GFP mice, compared to WT-GFP. The hepatomegaly observed was partially corrected by CYP46A1, as the levels of liver-to-body weight were significantly reduced by 10 % in NPC-CYP mice, compared to NPC-GFP. Overall, these results suggest that CYP46A1 expression has a positive impact on general health indicators of NPC animals.

3.3. *CYP46A1 ectopic expression promotes cholesterol redistribution in NPC mouse brain*

Due to the importance of CYP46A1 in brain cholesterol homeostasis, we further evaluated the impact of CYP46A1 expression on brain cholesterol levels. We started by quantifying total cholesterol levels in mouse cerebellum (Fig. 4A) and in cortex (Fig. 4B) using the Amplex® Red reagent. No significant differences in total cholesterol levels were observed between the different experimental groups, in the two brain regions. In fact, although NPC is characterized by cholesterol accumulation, it is also featured by a severe progressive neurodegeneration, which results in demyelination and loss of the associated cholesterol, which blocks out the unesterified cholesterol accumulation. Previous reports have detected a decrease in cholesterol levels in specific areas, such as the midbrain, brainstem, and spinal cord, where demyelination is most prominent [36–38].

Even though no differences were observed in the overall brain cholesterol content, since NPC disease is characterized by an intracellular accumulation of cholesterol, we assessed whether CYP46A1 was also able to revert the pathological accumulation of cholesterol in LE/L compartments. For that, parasagittal brain sections of WT-GFP, NPC-GFP, and NPC-CYP mice were stained with Filipin III, to label unesterified cholesterol (Fig. 4C).

As expected, all WT-GFP mice did not display any cholesterol accumulation (score = 0), while NPC-GFP mice showed an aggravated and localized cholesterol storage, which was translated to a high Filipin III score. Importantly, NPC-CYP mice exhibited a significant decrease in Filipin III staining when compared to NPC-GFP mice. This decrease in

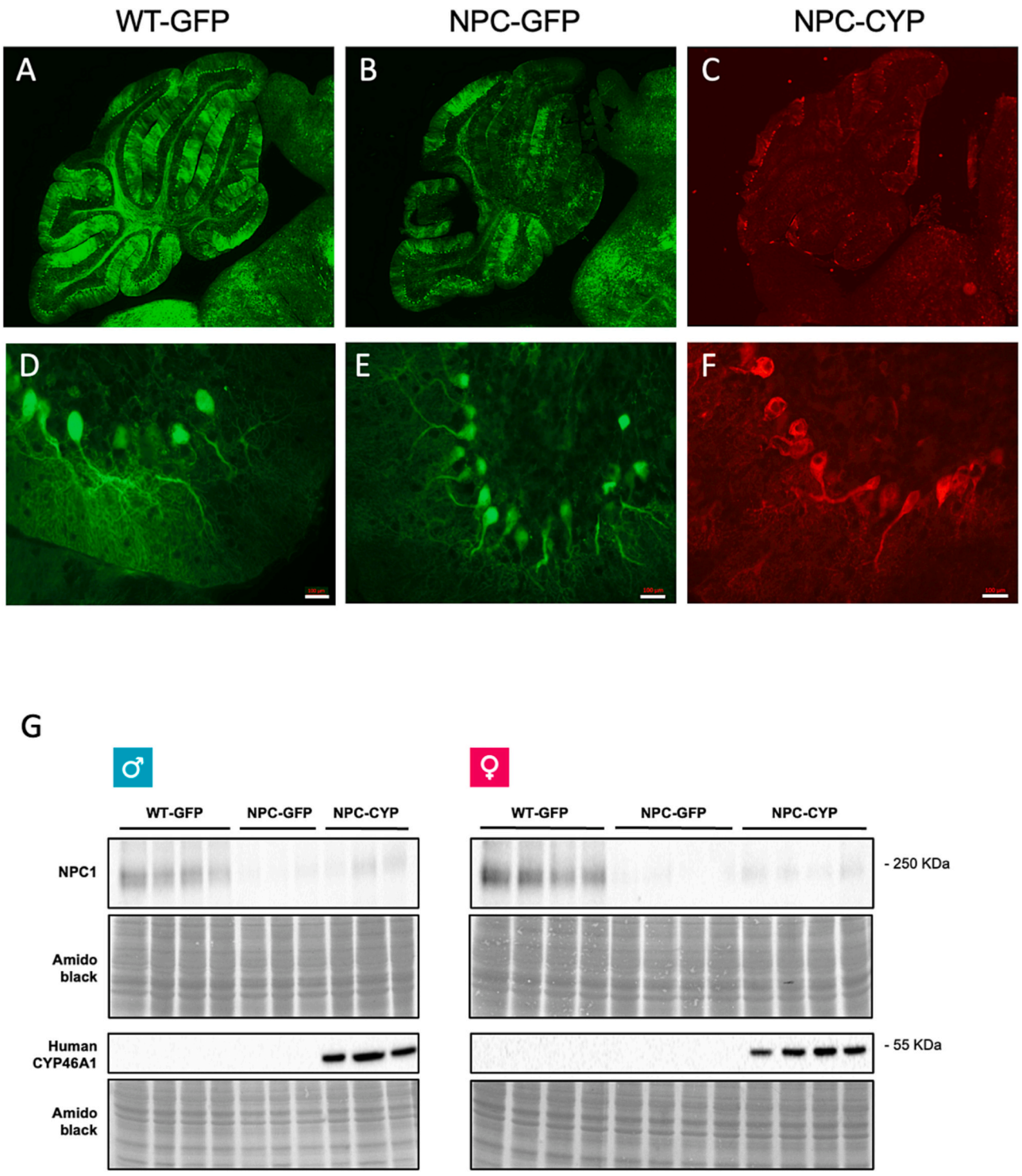

Fig. 2. Correct delivery of AAV encoding for GFP and CYP46A1 in mouse cerebellum. Wild-type mice received a retro-orbital injection with a dose of 5×10^{11} vg (viral genomes) of AAVPHP.eB-GFP (WT-GFP) vector, while Npc1tm(I1061T) mice received the same dose of AAVPHP.eB-GFP (NPC-GFP) or AAVPHP.eB-HA. CYP46A1 (NPC-CYP). Mice were injected at day 35 and sacrificed at 12 weeks of age. AVV-mediated GFP expression in WT-GFP and NPC-GFP mouse cerebellum, and AAV-mediated HA-tag expression in NPC-CYP mouse brain (Panel A, B and C, respectively). Microphotographs of more detailed Purkinje cells of cerebellar lobule X, expressing GFP (WT-GFP and NPC-GFP) or HA-tag (NPC-CYP) (scale bar: 100 μM) (Panel D, E and F, respectively). G) Western blot analysis of NPC1 and CYP46A1 in total extracts prepared from male (left panel) and female (right panel) mouse cerebellum using anti-NPC1 and anti-HA antibodies. Amido black staining was used as a loading control.

filipin-positive cells, of approximately 19 %, reflects the correcting effect of CYP46A1 expression on LE/L cholesterol accumulation (Fig. 4C).

To further dissect the effect of CYP46A1 ectopic expression on the correction of cholesterol homeostasis, we evaluated the transcriptional profile of genes involved in cholesterol metabolism. Total RNA was isolated from the cerebellum (Fig. 5) and cortex (Suppl. Fig. 2) of WT-GFP, NPC-GFP, and NPC-CYP mice, and the transcript levels of genes responsible for cholesterol synthesis and uptake, transport, and

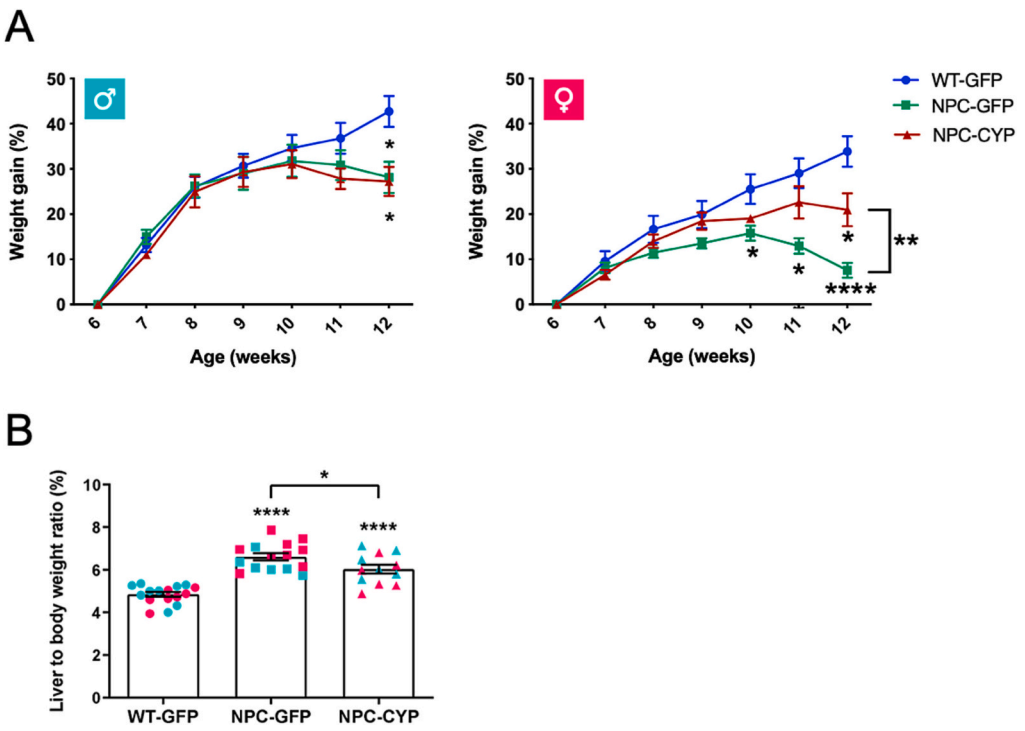

Fig. 3. Effect of CYP46A1 expression in body weight gain over time and liver to body weight ratio. Wild-type mice received a retro-orbital injection with a dose of 5×10^{11} vg (viral genomes) of AAVPHP.eB-GFP (WT-GFP) vector, while Npc1tm(I1061T) mice received the same dose of AAVPHP.eB-GFP (NPC-GFP) or AAVPHP.eB-HA.CYP46A1 (NPC-CYP). Mice were injected at day 35 and their weight was tracked weekly until 12 weeks of age. (A) Body weight gain of male (left panel) and female mice (right panel) presented as % of weight gain over 6-week-old weight. (B) Liver to body weight ratio (shown in percentage). Blue dots represent male mice and pink dots represent female mice. Statistical analysis was performed by ANOVA one-way tests followed by Tukey's multiple comparisons test. Asterisks directly over a bar indicate a significant difference relative to WT-GFP. Asterisk in brackets represent significant differences for the indicated groups (*$p < 0.05$, **$p < 0.01$, ****$p < 0.01$).

esterification were quantified by RT-qPCR.

SREBP2 is a transcription factor and master regulator of genes involved in cholesterol uptake and synthesis, including those encoding for *Ldlr*, *Hmgcs1*, and *Hmgcr*. Therefore, we started by analyzing the mRNA of *Srebp2*. Although the NPC phenotype did not affect the mRNA levels of *Srebp2*, NPC-CYP animals displayed a significant 1.3-fold increase in *Srebp2* mRNA levels detected both in the cerebellum (Fig. 5A) and cortex (Suppl. Fig. 2). Additionally, an increase in the active/cleaved form of SREBP2 was also detected in the cortex of NPC-CYP animals (Fig. 5G), further suggesting an activation of the mevalonate pathway after CYP46A1 delivery to the brain.

Considering that the activation of this transcription factor is a complex regulatory program that requires processing and nuclear translocation of an inactive precursor that is synthesized in the ER, we characterized the effect of CYP46A1 on mRNA levels of SREBP2-target genes *Ldlr, Hmgcs1* and *Hmgcr*. As previously mentioned LDLR is a crucial player in cholesterol uptake, while HMGCR catalyzes mevalonate synthesis, the rate-limiting step in the cholesterol synthesis pathway, and HMGCS catalyzes the conversion of acetyl-CoA into HMG-CoA, its substrate. *Ldlr* mRNA was significantly decreased in the cerebellum of NPC-GFP mice, compared to WT-GFP (0.8-fold) (Fig. 5B), although a similar decrease was not observed in the cortex (Suppl. 2B). Interestingly, CYP46A1 ectopic expression could restore *Ldlr* mRNA levels, in the cerebellum to levels that were 1.3-fold increased relative to WT-GFP animals. Similarly, in the cortex, we could observe a significant increase of about 1.5-fold in *Ldlr* expression in NPC-CYP when compared with WT-GFP.

Regarding *Hmgcs1* and *Hmgcr*, a significant decrease in the mRNA levels of both genes was observed in NPC-GFP mouse cerebellum (Fig. 5C and D) and cortex samples (Suppl. Fig. 2C and D), compared to WT-GFP littermates (0.9- and 0.7-fold in the cerebellum, respectively, and 0.8-fold for both genes in the cortex). Both in the cerebellum and cortex, CYP46A1 ectopic expression was able to restore the expression levels of these genes to values similar to those found in WT-GFP mice. This increase occurs concomitantly with the increase in the *Srebp2* and *Ldlr* mRNA levels, previously described. Altogether, these results demonstrate that CYP46A1 is partially restoring SREBP2-mediated gene regulation in the brain of NPC animals, suggesting an improvement in the ER function as the cholesterol sensor of the cell.

Another mediator of cholesterol homeostasis is the membrane cholesterol transporter ABCA1, which represents an important pathway for excess cellular cholesterol efflux. In the brain, ABCA1 is particularly abundant in Purkinje cells [39]. Our results show a significant increase in *Abca1* mRNA levels in NPC-GFP mice, in comparison to WT-GFP littermates (2.5-fold) (Fig. 5E). Again, CYP46A1 ectopic expression partially reverted this increase, leading to a decrease of approximately 28 % in NPC-CYP mice. Transcript levels of cholesterol acyltransferase 1 (*Acat1*) were also assessed in the cerebellum, as this enzyme is responsible for the esterification of cholesterol for storage. NPC animals also had a significant 1.6-fold increase in *Acat1* mRNA levels, relative to WT-GFP, while CYP46A1 expression reverted this effect, leading to a 15 % downregulation in the mRNA levels of this gene (Fig. 5F).

Gene expression analysis confirmed an extensive dysregulation of cholesterol metabolism-related gene expression in this NPC animal model, that is characterized by a significant decrease in cholesterol synthesis and uptake, and an increase in cholesterol efflux and esterification. Importantly, CYP46A1 ectopic expression was able to partially revert these changes, suggesting its *in vivo* beneficial effect.

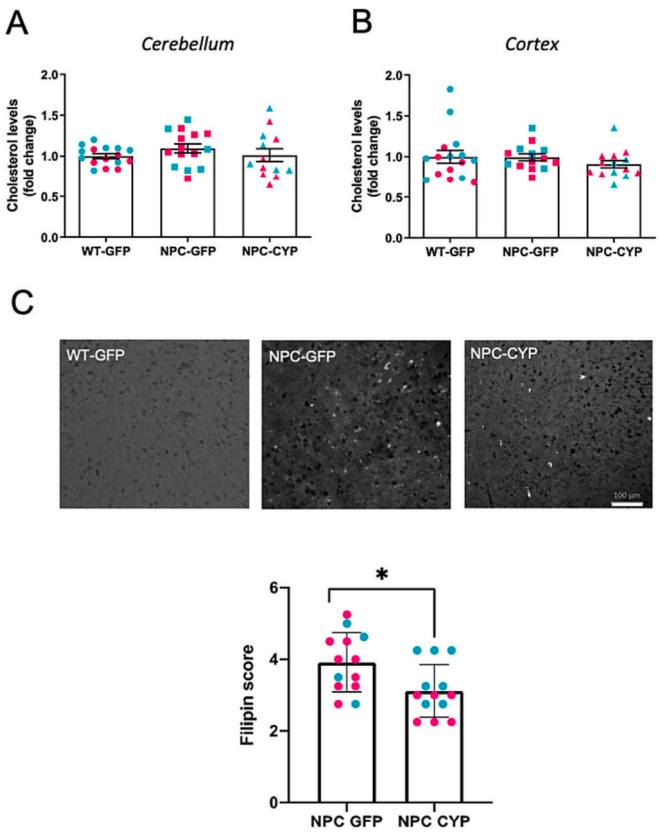

Fig. 4. CYP46A1 expression decreases accumulation of unesterified cholesterol in mouse brain. Wild-type mice received a retro-orbital injection with a dose of 5×10^{11} vg (viral genomes) of AAVPHP.eB-GFP (WT-GFP) vector, while Npc1tm(I1061T) mice received the same dose of AAVPHP.eB-GFP (NPC-GFP) or AAVPHP.eB-HA.CYP46A1 (NPC-CYP). Mice were injected at day 35 and sacrificed at 12 weeks of age. Cholesterol levels in mouse cerebellum (A) and cortex (B). Data represents mean values ± SEM and is presented as fold change to WT-GFP. (C) Filipin staining was analyzed in cortex slices in a double-blinded manner on a scale of 0–6, being 0 = no accumulation, 6 = extensive storage. Images (scale bar 100 µM) representative of the mean score of WT-GFP, NPC-GFP, and NPC-CYP mice (0, 4, and 3, respectively) are shown in upper panel, and data in the lower graphic is represented as mean values ± SEM. All WT-GFP animals have a score 0. Blue dots represent male mice and pink dots represent female mice. The Mann-Whitney test was performed. Asterisks directly over a bar indicate a significant difference relative to WT-GFP. Asterisk in brackets represent significant differences for the indicated groups (*$p < 0.05$).

3.4. CYP46A1 expression ameliorates lysosomal homeostasis in NPC mouse cerebellum and cortex

Since lysosomal dysfunction is a key feature in NPC disease [40], we determined in mouse cerebellum, the mRNA levels of *Tfeb*, which encodes a transcription factor that acts as a master regulator of lysosomal biogenesis, and its lysosomal target-genes cathepsin D (*CtsD*) and lysosomal-associated membrane protein 1 (*Lamp1*), as well as the autophagy gene *Sqstm1*, which encodes for sequestome 1/p62 (Fig. 6A).

Although the mRNA levels of *Tfeb* and *Lamp1* were unchanged in the cerebellum of NPC-GFP mice, we observed a significant increase in the expression levels of *CtsD* and *Sqstm1* of approximately 3.5 and 1.1, respectively, when comparing to WT-GFP. Interestingly, although CYP46A1 ectopic expression does not restore *CtsD* transcripts levels to the ones found in control animals, it induces a significant decrease of approximately 30 % when compared to NPC-GFP, while completely reverting the expression levels of *Sqstm1*.

The fact that CYP46A1 restores the expression levels of *Sqstm1*, which encodes a protein that serves as a pivotal cargo receptor for the degradation of ubiquitinated proteins, facilitating their removal *via* autophagic or proteasomal pathways, and the fact that NPC disease is also featured by autophagic flux impairment, we quantified the levels of native and lipidated LC3 (LC3-I and LC3-II, respectively) in NPC mouse brain (Fig. 6B). LC3 was not detected in cerebellum. In the cortex, NPC-GFP male and female mice showed a significantly increase of about 3.5- and 9.5-fold in LC3-II/I ratio, respectively, when compared with WT-GFP animals. Interestingly, CYP46A1 ectopic expression in females led to a significant decrease of approximately 30 % in LC3 II/I ratio when comparing to NPC-GFP mice. A similar tendency was observed in males, however no significant differences in the LC3-II/I ratio were detected when comparing NPC-GFP and NPC-CYP male mice.

The downregulation of *Ctsd* and *Sqstm1*, and the decrease in LC3-II/I ratio after CYP46A1 expression suggests an improvement of the intracellular trafficking when cholesterol homeostasis is re-established.

3.5. Effect of CYP46A1 ectopic expression on neuroinflammatory hallmarks of NPC disease

Neuroinflammation is one of the hallmarks of NPC disease, being the cerebellum one of the most affected regions, as evidenced by microglia activation, which is an important contributor to neurodegeneration in NPC1 [41]. Therefore, the effect of CYP46A1 ectopic expression on the mRNA levels of classic pro- and anti-inflammatory markers was assessed in NPC mouse cerebellum (Fig. 7).

Microglia activation was first confirmed in NPC mouse cerebellum by the significant increase of approximately 14.3, 3.7, 4.1, 3.7 and 8-fold in the mRNA levels of the microglial response markers integrin subunit alpha X (*Itgax*) (Fig. 7A), cluster of differentiation 68 (*Cd68*) (Fig. 7B), lysosomal-associated protein transmembrane 5 (*Laptm5*) (Fig. 7C), C-X3-C motif chemokine receptor 1 (*Cx3cr1*) (Fig. 7D), and triggering receptor expressed on myeloid cells 2 (*Trem2*) (Fig. 7E), respectively, when compared to the WT littermates. Interestingly, the increase in *Itgax* and *Cd68* expression levels was significantly reverted by CYP46A1 ectopic expression, leading to a decrease of approximately 27 % in the mRNA levels of those markers. Regarding microglia markers that typically indicate an anti-inflammatory response, the transcript levels of arginase 1 (*Arg1*) and transforming growth factor b (*Tgfb1*) were also quantified. ARG1 is a marker of anti-inflammatory microglia activation profile that is usually associated with tissue repair and phagocytosis [42]. Interestingly, although *Arg1* transcript levels observed in NPC-GFP mice were similar to those found in WT-GFP, CYP46A1 ectopic expression led to a significant increase of 1.5-fold in NPC-CYP mice, compared to NPC-GFP (Fig. 7F). Similarly, the mRNA levels of *Tgfβ,* a cytokine also produced when the microglia activation profile is anti-inflammatory, and involved in healing [42], did not register differences from WT-GFP to NPC-GFP mice (Fig. 7G). However, as for *Arg1* levels, a significant increase of 1.5-fold was observed in NPC-CYP mouse *Tgfβ* levels, compared to WT-GFP. These results suggest that CYP46A1 may have a positive impact in the neuroinflammatory phenotype of NPC disease.

The cerebellar microglial activation in NPC mice was accompanied by an increase in the mRNA levels of the pro-inflammatory cytokines interleukin (IL)-1β (*Il1β*) (Fig. 7H) and tumor necrosis factor alpha (*Tnfa*) (Fig. 7I) when compared to WT-GFP. However, no changes were observed after CYP46A1 ectopic expression. Interestingly, significant differences in the levels of *Il-1β* were observed between NPC-GFP male and female mice, since female NPC-GFP mice presented significantly higher transcript levels (1.4-fold) when compared to male NPC-GFP mice (Fig. 7H). This sex-specific differences were not detected for the other genes analyzed.

In response to damage-associated molecular patterns released from injured cells, microglia produce reactive oxygen species, leading to an elevation and sustained presence of these reactive species in disease conditions [43]. Therefore, we analyzed the mRNA levels of glutathione peroxidase 1 (*Gpx1*) (Fig. 7J) and heme oxygenase (*Hmox1*) (Fig. 7K),

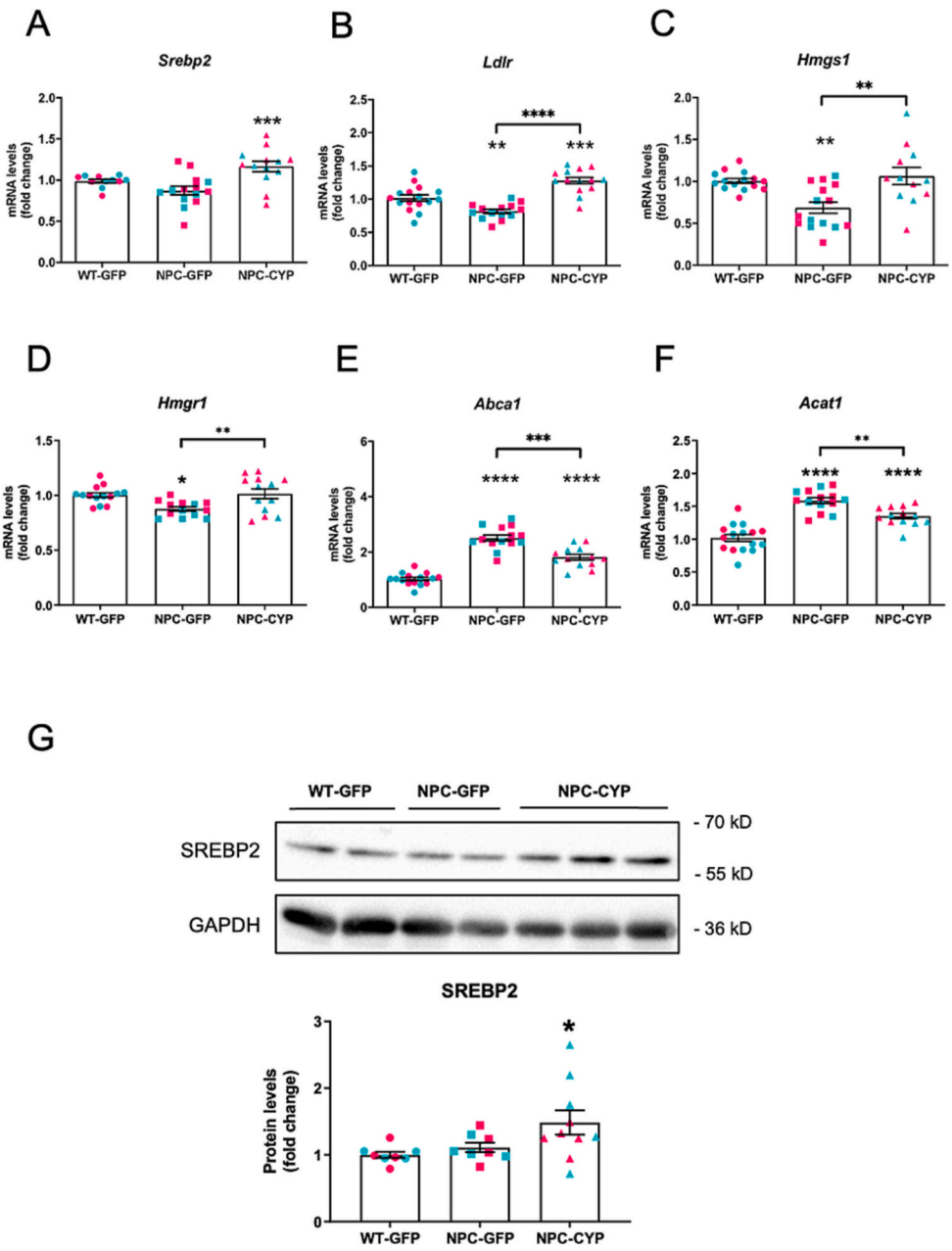

Fig. 5. CYP46A1 ectopic expression in NPC mouse cerebellum restores the mRNA levels of genes involved in cholesterol homeostasis. Wild-type mice received a retro-orbital injection with a dose of 5×10^{11} vg (viral genomes) of AAVPHP.eB-GFP (WT-GFP) vector, while Npc1tm(I1061T) mice received the same dose of AAVPHP.eB-GFP (NPC-GFP) or AAVPHP.eB-HA.CYP46A1 (NPC-CYP). Mice were injected at day 35 and sacrificed at 12 weeks of age. mRNA was extracted from cerebellum samples and transcript levels were measured by RT-qPCR using ribosomal protein large subunit 19 (*Rpl19)* and *Rpl29* as reference genes. mRNA levels of *Srebp2* (A), *Ldlr* (B), *Hmgcs1* (C), *Hmgcr* (D), *Abca1* (E), and *Acat1* (F) were calculated and plotted as a fold change over the average mRNA levels detected in WT-GFP mouse samples and represented as mean values ±SEM. G) SREBP2 protein levels in NPC mouse brain. Cortex protein extracts were analyzed by Western blot using an anti-SREBP2 antibody. GAPDH was used as loading control. Representative images are shown in the upper panel, and protein levels were quantified and plotted as percentage over the average protein levels detected in NPC-GFP mice and represent mean values ± SEM. Blue dots represent male mice and pink dots represent female mice. Asterisks directly over a bar indicate a significant difference relative to WT-GFP. Asterisk in brackets represent significant differences for the indicated groups (*$p < 0.05$, **$p < 0.01$, ***$p < 0.001$, ****$p < 0.0001$).

and observed a significant increase of about 1.2- and 2.3-fold, respectively, in NPC-GFP mouse cerebellum. Notably, ectopic expression of CYP46A1 halts the increase in *Gpx1* levels.

Overall, CYP46A1 ectopic expression in NPC mice corrects the observed increase in mRNA levels of some microglial response markers, such as *Cd68* and *Itgαx*, while it does not affect the expression of pro-inflammatory cytokines such as *Tnfα* and *Il-1β*. Interestingly, CYP46A1 expression significantly up-regulates the expression levels of *Arg1* and *Tgfβ*. Altogether, our results suggest that concomitant with the correction of cholesterol homeostasis, CYP46A1 may decrease neuroinflammation.

Since the gene expression analysis suggests that CYP46A1 ectopic expression is promoting alterations in the microglia profile in NPC mice, microglia activation was further analyzed in specific regions of the mouse cerebellum, based on Ionized calcium-binding adaptor protein-1 (IBA-1) immunostaining. IBA-1 is a actin-binding protein expressed specifically and constitutively in all microglia phenotypes [44]. It is extensively used as an immunohistochemical marker to identify both

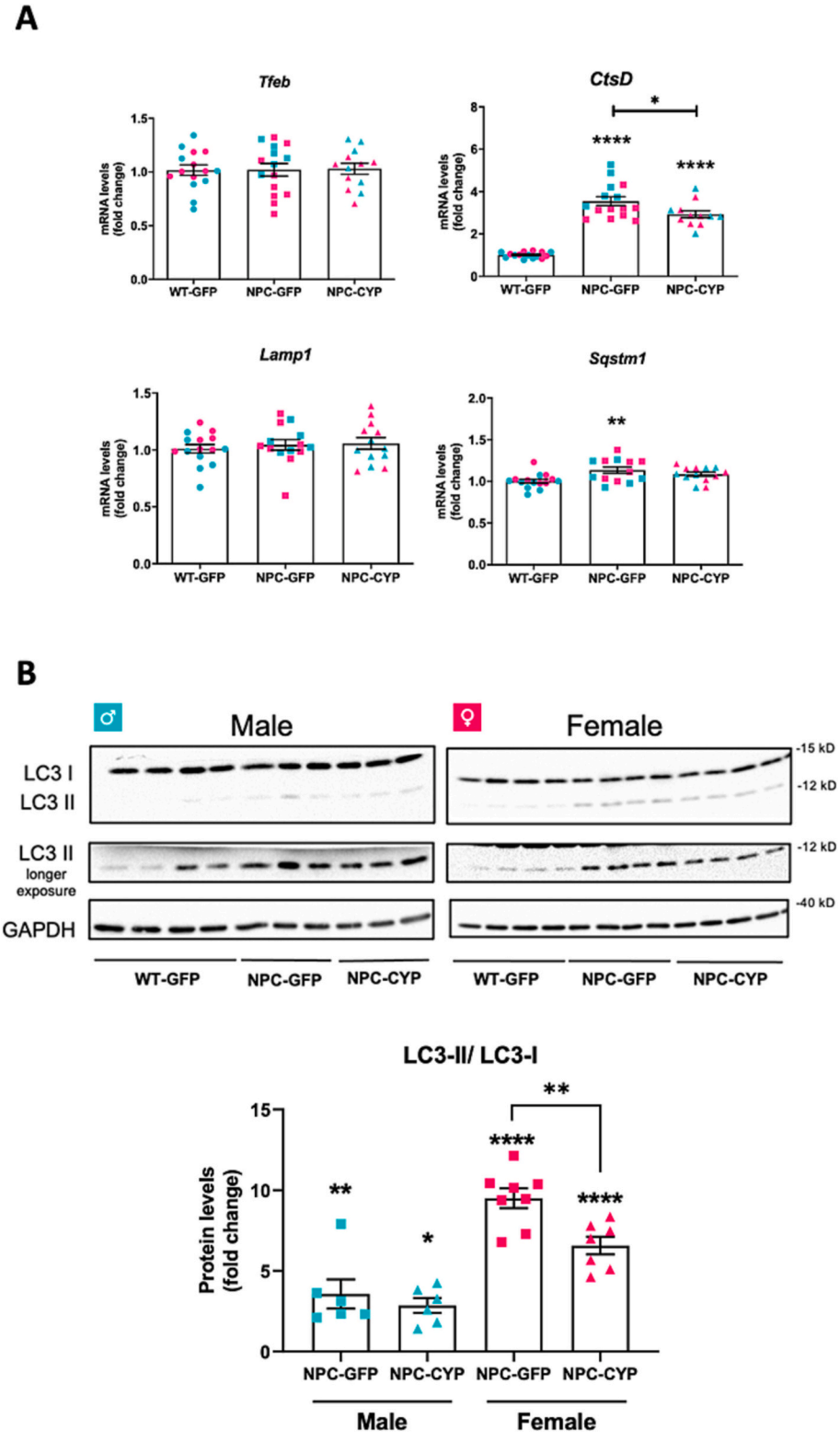

(caption on next page)

Fig. 6. CYP46A1 expression partially ameliorates lysosomal homeostasis in NPC mouse cerebellum and cortex. Wild-type mice received a retro-orbital injection with a dose of 5×10^{11} vg (viral genomes) of AAVPHP.eB-GFP (WT-GFP) vector, while Npc1tm(I1061T) mice received the same dose of AAVPHP.eB-GFP (NPC-GFP) or AAVPHP.eB-HA.CYP46A1 (NPC-CYP). Mice were injected at day 35 and sacrificed at 12 weeks of age. A) mRNA was extracted from cerebellum samples and mRNA levels of *Ctsd*, *Ctsf, Lamp1*, and *Tfeb* were measured by RT-qPCR using ribosomal protein large subunit 19 (*Rpl19)* and *Rpl29* as reference genes. Expression levels were calculated and plotted as fold induction over the average mRNA levels detected in WT-GFP mouse samples and represented as mean values ± SEM. B) Lipidation of Microtubule-associated protein 1A/1B-light chain 3 (LC3) in NPC mouse brain. Cortex protein extracts were analyzed by Western blot analysis using an anti-LC3 antibody. GAPDH was used as loading control. The immunoblots shown are representative of the results obtained in different experiments for male and female mice (upper panel). Quantification of the LC3-II/LC3-I ratio is represented as fold induction mean values ±SEM over WT-GFP (lower panel). One-way ANOVA, followed by Tukey's multiple comparisons test or Kruskal-Wallis test followed by Dunn's multiple comparisons test were performed Blue dots represent male mice and pink dots represent female mice. Asterisks directly over a bar indicate a significant difference relative to WT-GFP. Asterisk in brackets represent significant differences for the indicated groups ($*p < 0.05$, $**p < 0.01$ and $****p < 0.0001$).

ramified and activated microglia, particularly when there is robust microglial activation or a notable increase in microglia numbers. This is the case of NPC-GFP cerebellum where we could observe, in all the cerebellar regions analyzed, a clear increase in IBA-1 staining and in microglia cell body size. Fig. 8 show representative images of IBA-1 immunostaining in the deep nuclei (Fig. 8A), the inner granular (Fig. 8B), and the molecular layer (Fig. 8C) of the IV-V cerebellar lobules. Since IBA-1 staining is negligible in WT-GFP brain, we set the mean value of IBA-1 fluorescence detected in NPC-GFP male mice as 100 %, and both sex-differences and the CYP46A1 effect were analyzed. Interestingly, we observed a marked sex-specific difference in IBA-1 immunostaining. Indeed, IBA-1 staining is 70 % lower in the granular layer and 60 % in the molecular layer in female NPC-GFP cerebellum when compared to the same regions in NPC-GFP male cerebellum. Although, the observed differences were not statistically significant in the deep nuclei, IBA-1 fluorescence was 50 % ($p = 0.05$) lower in females. Surprisingly, ectopic expression of CYP46A1 led to a significant decrease in IBA-1 staining, of approximately 70 % in the granular and of 50 % in the molecular layer, only in male mice. A similar decrease in IBA-1 staining of about 50 % ($p = 0.050$), was observed in male deep nuclei. No statistically significant differences were observed in IBA-1 staining between NPC-GFP and NPC-CYP female mice.

Furthermore, we quantified IBA-1 protein levels by Western blot analysis (Fig. 9). Since astrogliosis is also present in NPC [45], in parallel we determined the protein levels of the astrogliosis-related protein glial fibrillary acidic protein (GFAP) (Fig. 9), as well as the transcript levels of *Gfap* and apolipoprotein E (*ApoE*), that were determined by RT-qPCR (Fig. 10).

In agreement with IBA-1 immunostaining, we observed a striking increase in IBA-1 protein levels in NPC-GFP animals (Fig. 9A). As previously described, since IBA-1 levels are very low in the WT-GFP brain, we set the mean value of IBA-1 levels detected in NPC-GFP mice as 100 %, to assess CYP46A1 effect. Although in total cerebellar extracts we did not detect any significant effect of CYP46A1 expression on IBA-1 protein levels, a similar tendency to decrease was observed in males (Fig. 9B – left panel).

The same approach was used to determine the effect of CYP46A1 expression in astrogliosis (Fig. 9A and B - right panel). An evident increase in GFAP protein levels was detected in NPC-GFP cerebellum, compared to WT-GFP (Fig. 9A), while CYP46A1 expression could not reverse this effect (Fig. 9B – right panel).

Additionally, the cerebellum mRNA levels of *Gfap* and *ApoE* were significantly increased in NPC-GFP mice, compared to WT-GFP (11.3- and 3.2-fold, respectively), confirming glial activation. In the cerebellum, CYP46A1 was not able to revert this increase (Fig. 10A and B).

Consistent with protein and mRNA levels, increased astrocytic activation was observed in the NPC mouse parasagittal cerebellum sections stained for GFAP. The cerebellum regions observed by confocal microscopy, namely the deep nuclei and inner granular layer (Fig. 10C and D, respectively) registered a demarked increase in GFAP labeling in NPC-GFP mice, compared to WT-GFP, reflecting the expected astrocytic reactive changes in NPC mice. No evident differences were observed between NPC-GFP and NPC-CYP mice, suggesting that CYP46A1 ectopic expression does not recover the astrogliosis present in the cerebellum of NPC animals.

Bergmann glia (BG) fibers localized in the molecular layer of the cerebellum were also visualized by GFAP fluorescent labeling (Fig. 10E). Mutation of the NPC1 protein has been suggested to alter the normal pattern of BG differentiation, and defects in the BG morphogenesis have previously been described in the $Npc1^{nmf164}$ mouse model, which displayed BG with radial shafts that were distended and of unequal caliber, compared to WT littermates [46]. Indeed, we also observed this altered morphology when comparing NPC to WT mice, with enlarged radial fibers in NPC mice. As a correct development of BG is crucial for cerebellar function, including synaptic activity [47], it was assessed whether CYP46A1 expression would revert the pathologic alterations. However, no differences were observed comparing NPC-GFP and NPC-CYP mice.

3.6. *Effect of CYP46A1 ectopic expression on neuronal cell death in NPC disease*

Cerebellar ataxia, as a result of the severe loss of Purkinje neurons, is a cardinal symptom of NPC disease. The previously described beneficial effects of CYP46A1 expression in restoring brain cholesterol homeostasis and reducing neuroinflammation in NPC animals led us to evaluate if CYP46A1 would display a correcting effect on Purkinje cell density. For the visualization of the Purkinje cells, mouse parasagittal cerebellum sections were stained with Cresyl Violet, and the number of Purkinje cells per mm of cell layer length, of each cerebellar lobule was counted for the WT-GFP, NPC-GFP, and NPC-CYP mice (Fig. 11A and B). As expected, neuronal loss was evident in NPC mice, with a significant decrease in Purkinje cell density in NPC-GFP mice compared to WT-GFP littermates. This decrease was more striking in the anterior zone, which comprises the cerebellar lobules I-V, compared to the central zone, which includes the lobules IX-X. These region-specific differences result from the progressive neurodegenerative process where Purkinje cell loss starts from the anterior zone to the posterior zone [7]. Even though still noticeable, neuronal loss was less apparent in the lobules IX-X, where Purkinje cells were still mostly preserved in the later stages of the disease. Comparing the Purkinje cell density between NPC-GFP and NPC-CYP mice, surprisingly, there were no striking differences, indicating that CYP46A1 ectopic expression did not prevent the Purkinje cell degeneration.

A similar profile was observed in the thickness of the molecular layer (Fig. 11C). When compared with their WT-GFP littermates, NPC-GFP and NPC-CYP mice show a significant decrease in the thickness of the molecular layer in cerebellar lobes I-VIII. No significant differences were observed between NPC-GFP and NPC-CYP mice in this area. In lobes VI to IX statistical differences were observed only between WT-GFP and NPC-CYP. In lobe X, no significant differences were detected. Regarding the thickness of the granular layer, we did not observe any significant differences between the three experimental groups (Fig. 11D).

To further confirm Purkinje cell loss, we determined the mRNA levels *Calb1*, which encode calbindin, a protein belonging to the large superfamily of cytoplasmic calcium-binding proteins, expressed in the brain and particularly concentrated in the Purkinje cells [48] (Fig. 11E). In parallel, mouse parasagittal cerebellum sections were processed for immunofluorescent staining for calbindin (Fig. 11F). Our results show a

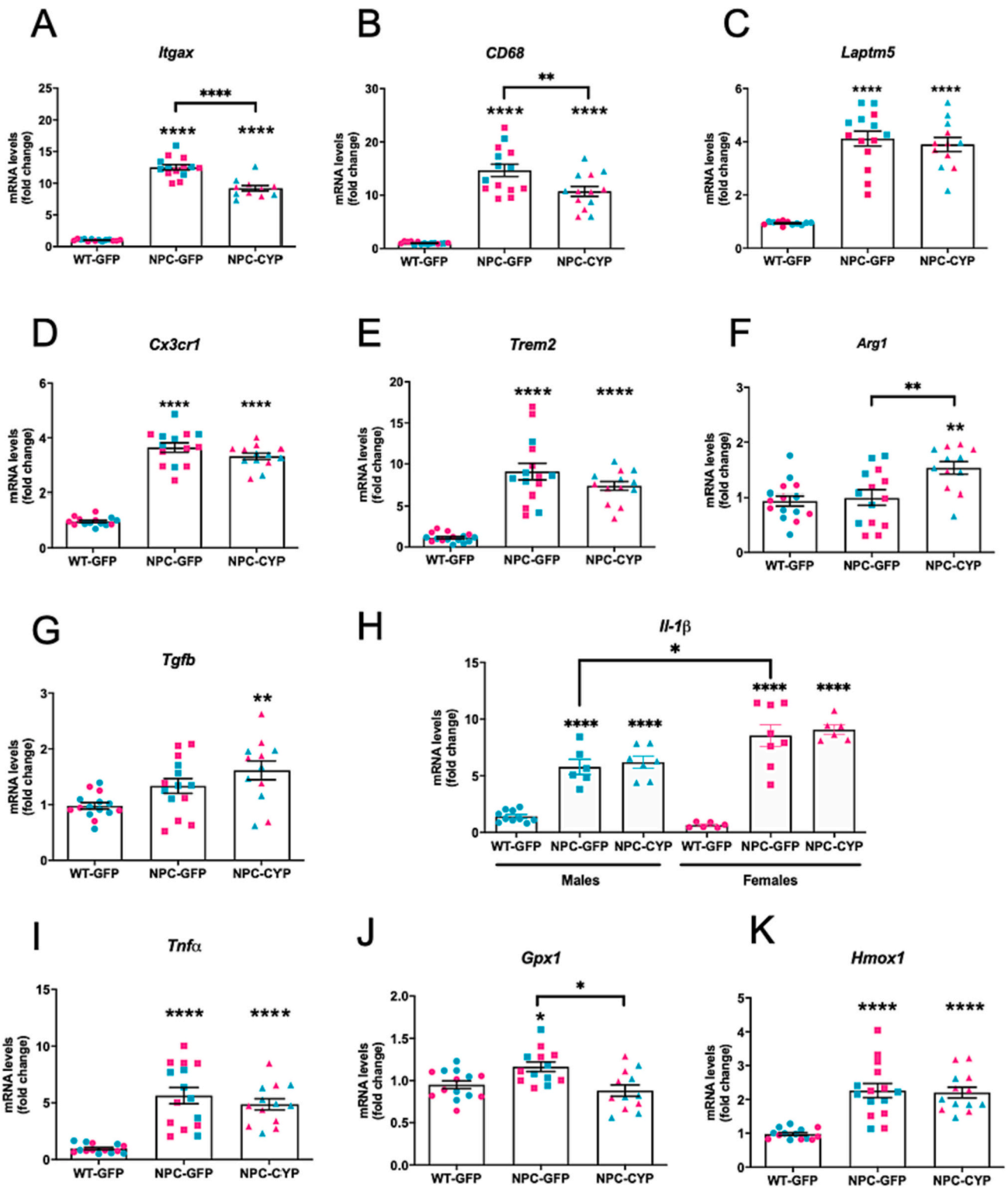

Fig. 7. Effect of CYP46A1 ectopic expression in NPC mouse cerebellum alters microglia phenotype. Wild-type mice received a retro-orbital injection with a dose of 5 $\times$ 10^{11} vg (viral genomes) of AAVPHP.eB-GFP (WT-GFP) vector, while Npc1tm(I1061T) mice received the same dose of AAVPHP.eB-GFP (NPC-GFP) or AAVPHP.eB-HA.CYP46A1 (NPC-CYP). Mice were injected at day 35 and sacrificed at 12 weeks of age. mRNA was extracted from cerebellum samples and transcript levels were measured by RT-qPCR using ribosomal protein large subunit 19 (*Rpl19)* and *Rpl29* as reference genes. mRNA levels of integrin subunit alpha X (*Itgax*) (A), cluster of differentiation 68 (*CD68*) (B), lysosomal-associated protein transmembrane 5 (*Laptm5*) (C) C-X3-C motif chemokine receptor 1 (*Cx3cr1*), (D) triggering receptor expressed on myeloid cells 2 (*Trem2*) (E), arginase 1 (*Arg1*) (F) transforming growth factor b (*Tgfb1*) (G), interleukin (IL)-1b (*Il1b*) (H), tumor necrosis factor (*Tnfa*) (I), glutathione peroxidase 1 (*Gpx1*) (J) and heme oxygenase (*Hmox1*) (K) were calculated and plotted as a fold change over the average mRNA levels detected in WT-GFP mouse samples and represented as mean values ±SEM. In the case of *Il1b* results are presented as fold change over the average mRNA levels detected in WT-GFP male mouse samples. Blue dots represent male mous and pink dots represent female mice. Asterisks directly over a bar indicate a significant difference relative to WT-GFP. Asterisk in brackets represent significant differences for the indicated groups (*$p < 0.05$, **$p < 0.01$, ***$p < 0.001$, ****$p < 0.0001$).

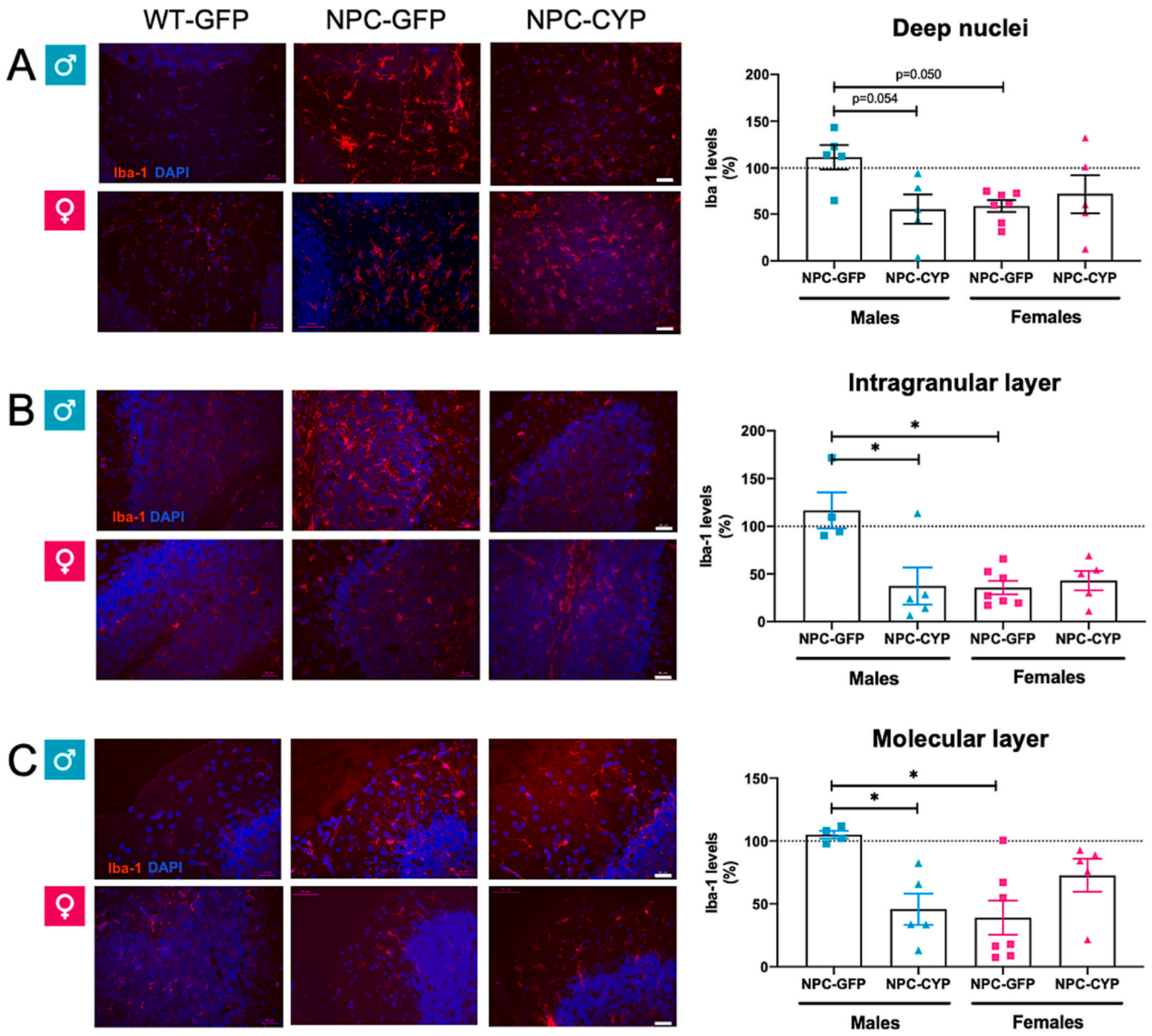

Fig. 8. Effect of CYP46A1 in the expression levels of the microglial activation markers Iba-1 in the cerebellar cortex. Wild-type mice received a retro-orbital injection with a dose of 5×10^{11} vg (viral genomes) of AAVPHP.eB-GFP (WT-GFP) vector, while Npc1tm(I1061T) mice received the same dose of AAVPHP.eB-GFP (NPC-GFP) or AAVPHP.eB-HA.CYP46A1 (NPC-CYP). Mice were injected at day 35 and sacrificed at 12 weeks of age. Parasagittal brain sections from these animals were immunostained with anti-Iba1 antibody (red) and nuclei were stained with DAPI (blue). Fluorescent microscopy photographs of the deep nuclei (A), and the intragranular (B) and molecular layers (C) of lobule IV-V. Iba-1 levels were quantified with Image J and the data presented in the graphics in the right panels represent mean values of fluorescence units ± SEM and is expressed as percentage, over mean values of relative fluorescence units observed in NPC-GFP male mice that were set at 100 % (scale bar: 20 μm). Blue dots represent male mice and pink dots represent female mice. Asterisks directly over a bar indicate a significant difference relative to WT-GFP. Asterisk in brackets represent significant differences for the indicated groups ($^*p < 0.05$).

striking and significant decrease in the expression levels of *Calb1* of approximately 85 %, which was not affected by CYP46A1 expression. In agreement with previous results, sections stained with the anti-calbindin antibody revealed a similar loss in Purkinje cell number, reflecting a demarked degeneration between NPC-GFP mice and WT-GFP littermates, which was not corrected by CYP46A1 ectopic expression.

3.7. Effect of CYP46A1 ectopic expression in Npc1$^{tm(I1061T)}$ mouse motor function

We further examined the effect of CYP46A1 ectopic expression on neurological disease progression in the mice using rotarod, open field and catwalk gait analysis (Fig. 12), which had been previously validated in NPC1 mouse models [30,49,50].

Regarding motor symptoms at 6 weeks of age, we observed the onset of a visible resting tremor in some Npc1$^{tm(I1061T)}$ mice, and in contrast to that previously described for this mouse model [30], we detected a significant decrease in rotarod retention time as early as at 6 weeks of age in NPC-GFP mice (Fig. 12A), when compared with WT-GFP. WT-GFP animals were able to maintain their balance on the rotating drum throughout the studied period. NPC-GFP and NPC-CYP animals showed a significant decrease in rotarod retention time over time, from an average of 380 and 347 s on week 6, to approximately 16 and 22 s on week 12, respectively. No significant differences were observed in retention time between NPC-GFP and NPC-CYP animals.

To further assess alterations in individual spontaneous locomotor

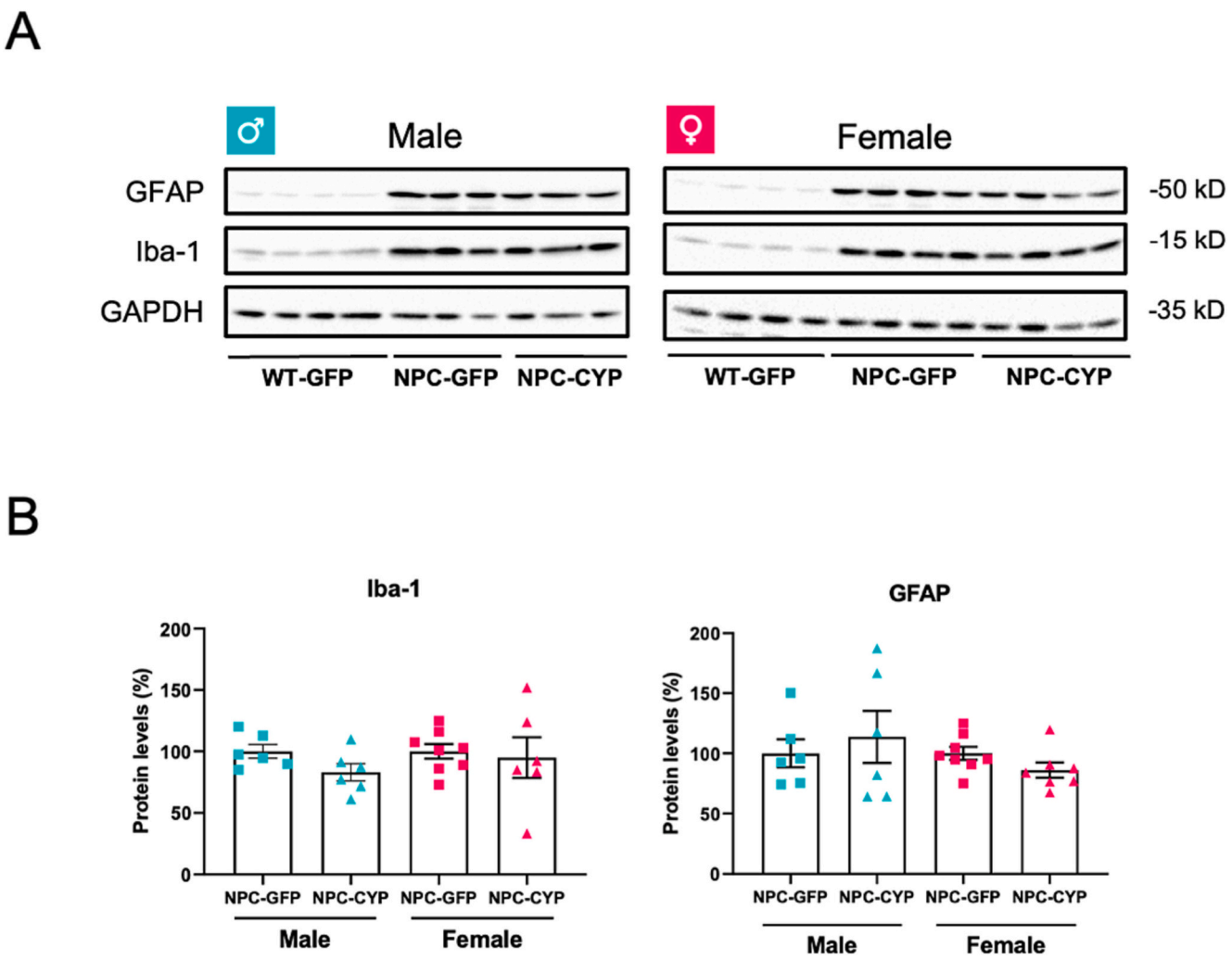

Fig. 9. Effect of CYP46A1 ectopic expression on neuroinflammation in NPC mouse cerebellum. Wild-type mice received a retro-orbital injection with a dose of 5×10^{11} vg (viral genomes) of AAVPHP.eB-GFP (WT-GFP) vector, while Npc1tm(I1061T) mice received the same dose of AAVPHP.eB-GFP (NPC-GFP) or AAVPHP.eB-HA.CYP46A1 (NPC-CYP). Mice were injected at day 35 and sacrificed at 12 weeks of age. Total extracts were prepared from mouse cerebellum samples and analyzed by Western Blot using anti-GFAP and anti-Iba-1 antibodies. GAPDH was used as loading control. A) The immunoblots shown are representative of the results obtained for males and females. B) Protein levels were quantified and plotted as percentage over the average protein levels detected in NPC-GFP male and female mouse and represent mean values ± SEM.

activity at 12 weeks of age, the Open Field Test was used. In agreement with results obtained with the rotarod motor test, the data obtained show clear motor deficits. We found a significant decline on average velocity, total distance travelled, and number of crossings of the arena (Fig. 12B). Similarly, the percentage of time the animals spent moving fast decreased, while the percentage of time moving slowly increased. Resting time was not affected between experimental groups. No significant differences were observed between NPC-GFP and NPC-CYP animals.

Catwalk gait analysis at 12 weeks of age indicated that both NPC-GFP and NPC-CYP mice showed a significant decrease on average left and right hind and forelimbs stride length. There were no significant differences between NPC-GFP and NPC-CYP animals at this age (Fig. 12C).

Together, our findings demonstrate that CYP46A1 ectopic expression at the time of onset of NPC symptoms did not preserve neurological and motor function in Npc1$^{tm(I1061T)}$ mice.

4. Discussion

Considering the role of CYP46A1, the neuron-specific enzyme that catalyzes the major brain cholesterol elimination pathway, we hypothesized that overexpression of CYP46A1 was beneficial in NPC. Herein, we showed that ectopic expression of CYP46A1 in fibroblasts of NPC patients carrying different mutations, namely the NPC1I1061T mutation, the most prevalent in human patients encoding a misfolded protein with reduced half-life that is targeted for ER-mediated degradation, led to a significant amelioration of the cholesterol accumulation in LE/L.

To understand if CYP46A1 could improve the pathological NPC phenotype *in vivo*, the NPC1$^{tm(I1061T)}$ mouse model was used [30]. This model has the knock-in of the NPC1I1061T mutation, and the pathologic features observed in animals, recapitulate those in human NPC disease, including the characteristic decreased motor coordination, brain lesions, particularly in the cerebellar area leading to Purkinje cell death, dendritic and axonal abnormalities, lipid storage, and premature death.

In order to pursue a clinically effective gene therapy approach, we used the recently developed AAVPHP.eB-HA.CYP46A1 vector that can cross the blood brain barrier, and therefore can be injected in the retro-orbital region, without the need for the invasive form of surgical intervention, such as the stereotaxic injection. Our results showed high levels of expression of the transgene in the cerebellum and cortex of NPC mice.

General health indicators such as body weight loss and liver-to-body

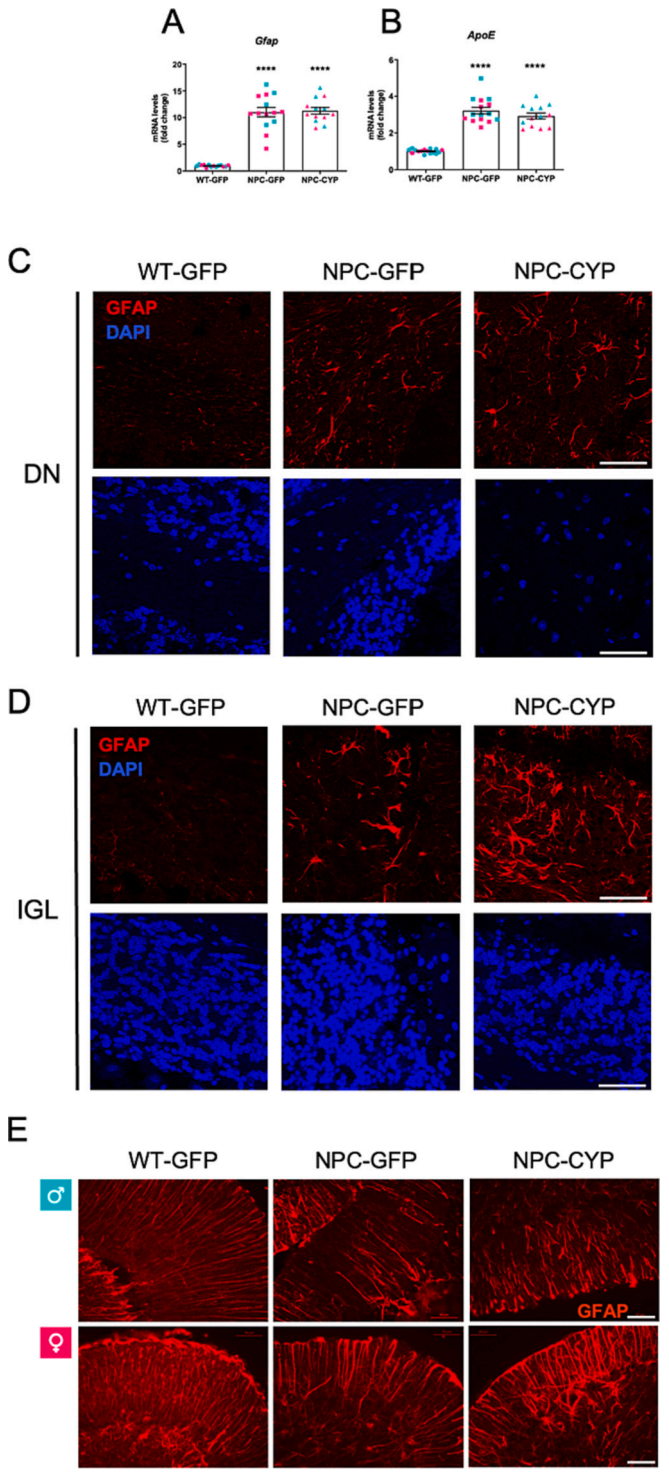

(caption on next column)

Fig. 10. CYP46A1 ectopic expression in NPC mouse cerebellum does not affect astrogliosis. Wild-type mice received a retro-orbital injection with a dose of 5×10^{11} vg (viral genomes) of AAVPHP.eB-GFP (WT-GFP) vector, while Npc1tm (I1061T) mice received the same dose of AAVPHP.eB-GFP (NPC-GFP) or AAVPHP.eB-HA.CYP46A1 (NPC-CYP). Mice were injected at day 35 and sacrificed at 12 weeks of age. mRNA was extracted from cerebellum samples and mRNA levels were measured by RT-qPCR using ribosomal protein large subunit 19 (*Rpl19)* and *Rpl29* as reference genes. mRNA levels of glial fibrillary acidic protein (*Gfap*) (A) and apolipoprotein (*ApoE*) (B), were calculated and plotted as a fold change over the average mRNA levels detected in WT-GFP mouse samples and represented as mean values ±SEM. Asterisks directly over a bar indicate a significant difference relative to WT-GFP (C-E) Astrocyte morphology/activation in parasagittal brain sections immunostained with anti-GFAP antibody (red), stained with DAPI for nuclei localization (blue). Representative confocal microscopy fluorescent photographs of astrocyte in the deep nuclei (DN) (C), intragranular (IGL) layer of lobules IV-V (D) and Bergmann glia fibers in the molecular layer of lobule lobules IV-V (E) (****$p < 0.0001$; scale bar: 50 μm).

weight show that CYP46A1 has a beneficial role in ameliorating the NPC phenotype. Indeed, female NPC-CYP mice maintained their body weight gain from week 10 onwards, in contrast to NPC-GFP mice. Loss of body weight is due to motor disabilities and altered metabolic factors, so further studies should determine why this difference was not observed in male mice. Nevertheless, CYP46A1 significantly reversed the pathological increase in liver-to-body weight observed in both female and male NPC mice.

Strikingly, CYP46A1 expression partially re-established cholesterol homeostasis in Npc1$^{tm(I1061T)}$ mice. Total cholesterol levels were determined in NPC mouse cerebellum and cortex, but no differences were observed between the experimental groups. In fact, although NPC is characterized by cholesterol accumulation, it is also featured by severe progressive neurodegeneration, which results in demyelination and loss of the associated cholesterol that blocks out the unesterified cholesterol accumulation. Indeed, previous reports have detected a decrease in cholesterol levels in specific areas, such as the midbrain, brainstem, and spinal cord, where demyelination is most prominent [36–38]. Nevertheless, the characteristic intracellular unesterified cholesterol accumulation, confirmed by filipin staining on mouse parasagittal brain sections, and consistent to that previously described in this model [30,51], was significantly decreased after CYP46A1 ectopic expression, suggesting a redistribution of the accumulated cholesterol within the cells, which is in agreement with our *in vitro* data. Gene expression analysis confirmed the hypothesis of improving intracellular cholesterol mobilization. NPC phenotype was characterized by a significant decrease in cholesterol synthesis (*Hmgr* and *Hmgs1*) and uptake (*Ldlr*), along with increased cholesterol efflux (*Abca1*) and esterification (*Acat1*), but CYP46A1 ectopic expression was able to restore the mRNA levels to those in WT-GFP mice. The fact that cholesterol homeostasis regulators such as SREBP2 and LXR responded to CYP46A1 expression further suggests that CYP46A1 improves cholesterol homeostasis in the brain, by promoting the egress of cholesterol from the LE/L compartments by an alternative pathway that is either independent of the NPC1 protein or works in parallel to the NPC1-mediated route. CYP46A1, through production of 24(*S*)-hydroxycholesterol could be promoting an ABCA1-mediated efflux of endolysosomal cholesterol, as overexpression of this transporter in NPC-deficient fibroblasts has been shown to reduce the accumulation of cholesterol [52]. Alternatively, CYP46A1 can be promoting a vesicle-mediated transport pathway, by increasing prenylation of Rab proteins. Interestingly, downregulation of NPC1 has been recently described in aged neurons, concomitantly with the accumulation of cholesterol in multivesicular bodies, which increased secretion of small extracellular vesicles as a protective mechanism [53], and with increased CYP46A1.

As cholesterol accumulation mainly occurs at the lumen and limiting membrane of LE/L, it results in enlarged lysosomes that present defects

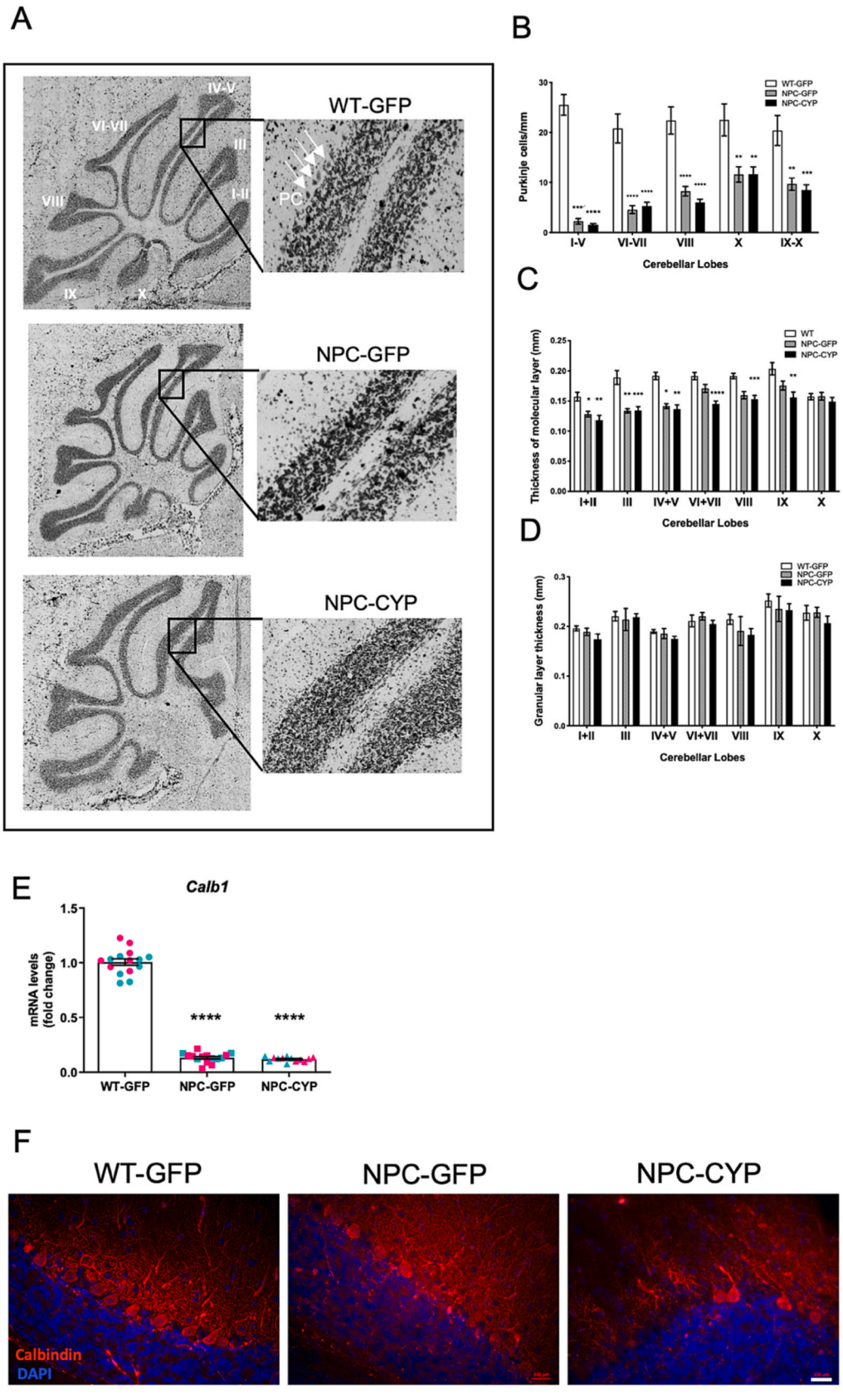

(caption on next page)

Fig. 11. CYP46A1 ectopic expression does not stall Purkinje cell death. Wild-type mice received a retro-orbital injection with a dose of 5×10^{11} vg (viral genomes) of AAVPHP.eB-GFP (WT-GFP) vector, while Npc1tm(I1061T) mice received the same dose of AAVPHP.eB-GFP (NPC-GFP) or AAVPHP.eB-HA.CYP46A1 (NPC-CYP). Mice were injected at day 35 and sacrificed at 12 weeks of age. A) Parasagittal brain sections from these animals were subjected to Cresyl Violet staining, allowing the visualization of Purkinje cells in the cerebellum. WT- GFP, NPC-GFP, and NPC-CYP Purkinje cells (PC) were counted manually, and the length of the Purkinje cells layers was measured in each cerebellar lobe, allowing the determination of the Purkinje Cell Density (B). The thickness of the molecular layers (ML) and granular layer (GL) are presented in panels (C) and (D), respectively. mRNA was extracted from cerebellum samples and transcript levels were measured by RT-qPCR using *Rpl19* and *Rpl29* as reference genes. mRNA levels of calbindin 1 (*Calb1*), was calculated and plotted as fold induction over the average mRNA levels detected in WT-GFP mouse samples (E). Parasagittal brain sections from these animals were subjected to calbindin and DAPI staining, as calbindin allows the visualization of Purkinje cells (F). Representative regions of lobule X of the calbindin-stained cerebellum of WT-GFP, NPC-GFP, and NPC-CYP mice are presented (scale bar: 50 μM). In graphics data are presented as mean values ± SEM. ANOVA one-way tests were performed followed by Tukey's multiple comparisons test. Asterisks directly over a bar indicate a significant difference relative to WT-GFP. ($^{*}p < 0.05$, $^{**}p < 0.01$, $^{***}p < 0.001$ and $^{****}p < 0.0001$ *vs* WT-GFP).

at a morphological, trafficking, and functional level [54]. Therefore, we assessed the effect of CYP46A1 ectopic expression in lysosomal function. In agreement with previous published data in the Npc1$^{-/-}$ mouse model [40], we observed higher *Ctsd* expression levels that were partially corrected in NPC-CYP mice. Lysosomal dysfunction is often associated with defects in autophagy. Studies have demonstrated that defective autophagy in NPC disease is linked to cholesterol accumulation. This occurs since the maturation of autophagosomes is hindered due to faulty amphisome formation caused by a malfunction in the SNARE machinery. However, the lysosomal proteolytic function remains unaffected [55]. To determine the status of autophagic activity in brains of NPC-GFP mice, levels of LC3 were assessed in the cortex. LC3 undergoes modification through a process similar to ubiquitination. Initially, LC3 is cleaved at its carboxyl terminal, resulting in LC3-I. Subsequently, autophagy-related 7 (Atg7) and Atg3 further modify LC3-I, converting it into a membrane-bound form known as LC3-II [56]. This modification of LC3 is crucial for the formation of autophagosomes, making LC3-II a widely utilized marker for these structures. Our results show an increase in the LC3-II/LC3-I ratio that is probably not due to increased autophagosome synthesis, but rather caused by decreased degradation of autophagosomes. Interestingly, the LC3-II/LC3-I ratio decreased in the cortex of AAV-CYP46A1 injected Npc1$^{tm(I1061T)}$ mice, indicating that CYP46A1 expression can partially normalize autophagic flux in NPC mouse brain. Interestingly, the unblock of autophagic flux occurs concomitantly with the effect on cholesterol homeostasis and increased *Srebp2* mRNA and protein levels. Studies have revealed that SREBP2 directly activates autophagy genes when cellular sterol levels are depleted, a condition that induces both autophagy and increased nuclear SREBP2 levels. Moreover, knocking down SREBP2 during nutrient depletion has been shown to reduce autophagosome formation and impair the lipid droplet association of the autophagosome-targeting protein LC3 [57].

Microgliosis is the first evidence of neuroinflammation in NPC, and previous studies have suggested that targeting microglia decreases the rate of neuronal loss, slowing disease progression and therefore increasing the longevity of NPC mice [41]. Our gene expression analysis in the Npc1$^{tm(I1061T)}$ model is in accordance with the microglia activation profile previously described after single-cell transcriptome analysis for Npc1$^{-/-}$ mice [58]. The NPC-associated microglia profile was characterized by the upregulation of markers associated with microglial response *Cd68*, *Itgax*, *Cx3cr1*, indicators of the NPC microglia reactive amoeboid state, as well as of pro-inflammatory cytokines *Tnfα*, and *Il-1β*. Interestingly, sex-specific differences were observed in the transcript levels of *Il-1β,* which had not been previously described in this model. Nevertheless, microglia have been shown to respond to environmental challenges in a sex- and time-dependent manner [59]. Regarding microglia markers that typically indicate an anti-inflammatory response, *Arg1* and *Tgfβ* mRNA levels were not altered in the NPC phenotype. Levels of the modulator of microglia function *Trem2* also registered a significant increase in NPC mice. CYP46A1 ectopic expression recovered the dysregulation of some microglia markers in NPC mice, as *Cd68* and *Itgax* levels, while promoting the expression of markers of anti-inflammatory microglia profile, by significantly up-regulating *Arg1* and *Tgfβ*. Overall, these results suggest CYP46A1 expression is associated with a more neuroprotective and healing activation profile. The effect of CYP46A1 towards microglial activation was further confirmed by the decrease in IBA-1 levels observed in NPC mouse brain. Here, again, we observed clear sex-dependent differences in IBA-1 immunostaining, since the increase in IBA-1 protein levels in the NPC cerebellum, is more striking in male brains. CYP46A1 expression decrease IBA-1 levels in both the intragranular and molecular layers of lobules IV-V in the cerebellum of NPC male mice, whilst no effect was registered in females.

Finally, as the neurodegenerative cascade initiated by microglia activation in NPC leads to astrocytosis, the effect of CYP46A1 was assessed on this neuroinflammatory hallmark. Surprisingly, the increase in cerebellar astrocytic activation observed in Npc1$^{tm(I1061T)}$ mice was not recovered by CYP46A1. Interestingly, specific transgenic astrocytic expression of wild-type NPC1 protein can ameliorate the disease state of Npc1$^{-/-}$ mice, increasing survival nearly 2.5 times, which strongly implicates astrocytes in neurodegeneration [60]. Our results suggest that NPC1 loss in astrocytes is by itself an important factor affecting cell reactivity, and that cholesterol sequestration within astrocytes can further trigger the inflammatory response, impair neuronal function, and contribute to the progression of neurodegeneration. However, we cannot exclude the hypothesis that CYP46A1 could be delaying astrogliosis and consequently Purkinje cell death.

Although crucial pathological features of the disease including cholesterol homeostasis, lysosomal and autophagy dysfunction, as well as microglia activation, were improved in response to CYP46A1 ectopic expression, no ameliorations were observed regarding the NPC-characteristic Purkinje cell death in cerebellum and the consequent motor disabilities, at 12 weeks of age. It would be of interest to perform these analyses at an earlier age to evaluate if the observed improvement in neuroinflammation and cholesterol homeostasis can slow down the progression of Purkinje cell degeneration.

Our results are in apparent contradiction with the report of Mitroi et al. [61], where CYP46A1 activation by efavirenz treatment restored LTP and prevented lysosomal cholesterol accumulation, neuronal cell death and motor impairment in the NPC1^{nmf164} mouse model. The *nmf164* allele is a point mutation (D1005G mutation) in *Npc1*, which results in partial functional loss of the protein, similar to mutations commonly observed in patients [62]. Animals carrying this mutation have a slower progression of symptoms than *Npc1*-null mice and are a suitable model to study late-onset NPC. Despite the fact that the animal models used in both studies are phenotypically very similar, we cannot rule out the possibility that this could, at least in part, be the cause of the conflicting findings. Nevertheless, our findings demonstrate that only part of the observed beneficial effects of efavirenz treatment result from CYP46A1 activation, highlighting the importance of other targets when using low doses of this anti-HIV drug in neuropathological conditions, including Alzheimer's disease [63,64]. Unesterified cholesterol accumulation has frequently been indicated as the main cause of neuronal cell death in NPC and most developed drug screenings have been directed to LE/L cholesterol storage and modulation of cholesterol regulation. However, the fact that improving cholesterol homeostasis in neurons is not sufficient to halt Purkinje cell death has already been previously suggested. In addition to cholesterol, the NPC-affected LE/L

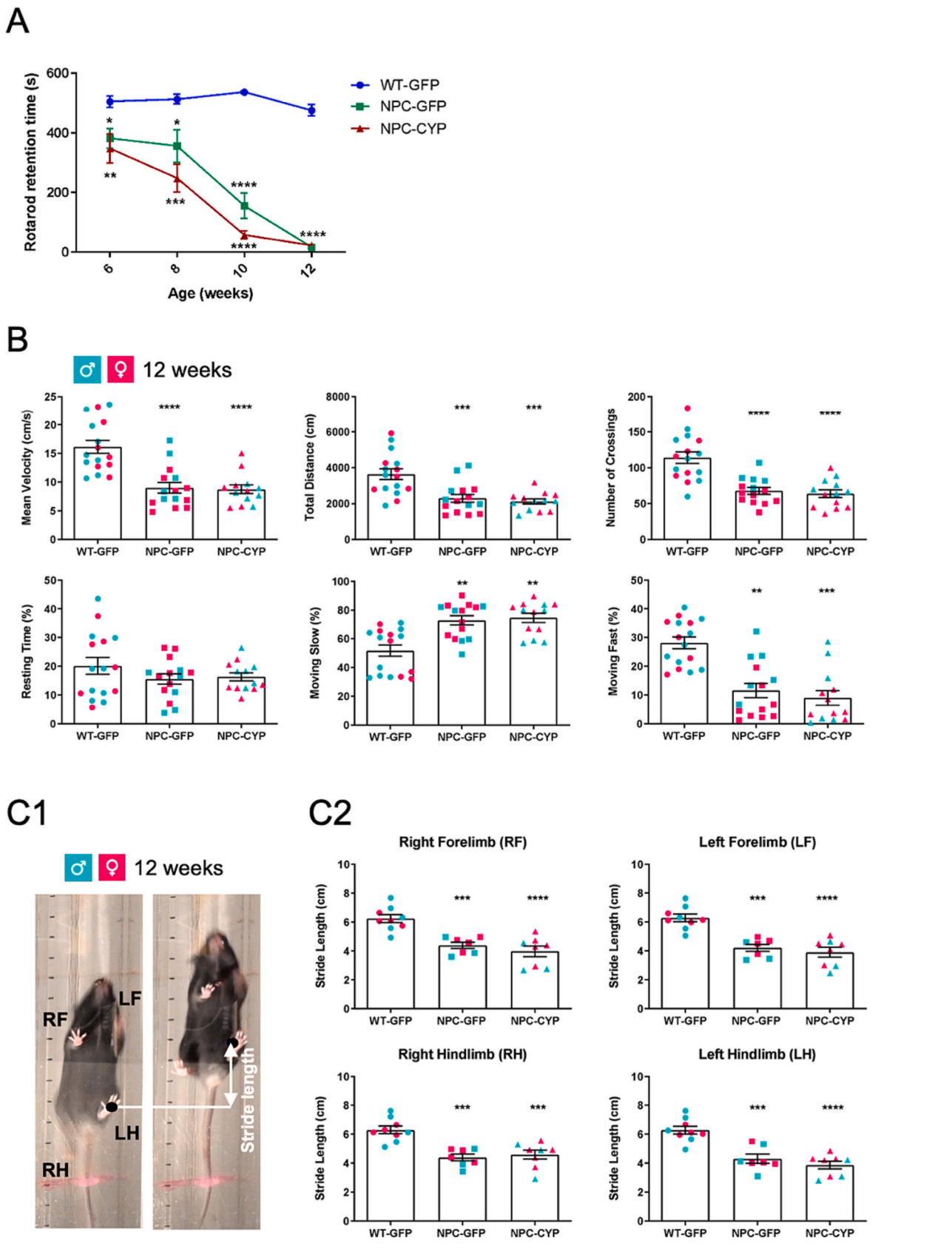

(caption on next page)

Fig. 12. Effect of CYP46A1 expression in mouse motor coordination and general locomotor activity. Wild-type mice received a retro-orbital injection with a dose of 5×10^{11} vg (viral genomes) of AAVPHP.eB-GFP (WT-GFP) vector, while Npc1tm(I1061T) mice received the same dose of AAVPHP.eB-GFP (NPC-GFP) or AAVPHP.eB-HA.CYP46A1 (NPC-CYP). Mice were injected at day 35 and rotarod motor test was performed every two weeks, from week 6 until week 12, and both catwalk and open field test were performed at week 12. A) Rotarod retention time was assessed in a constant 10 rpm rotating drum in two consecutive days and the best performance is presented for each time point. Values reported are the sum of the time spend on the rotarod for 3 consecutive attempts (s), of a maximum of 180 s per attempt. B) General locomotor activity at 12 weeks of age evaluated by the open field test. Each animal was placed in the center of the arena and allowed to freely walk for 5 min. Mouse movements were recorded and analyzed using the video-tracking software – SMART® allowing the determination of mean velocity, total distance travelled, number of crossings between the three different square zones, and the percentage of resting time and time spent walking slow or fast. C) Catwalk gait analysis at week 12. Each animal was placed individually in a transparent platform, where it was allowed to move freely for a maximum of 4 min. Animal locomotion was recorded allowing the determination of stride length (cm), as represented in C1, of left (LH) and right hindlimbs (RH) and left (LF) and right forelimbs (RF) (C2). Results are presented as mean value ± SEM and statistical analysis was performed by ANOVA one-way tests followed by Tukey's multiple comparisons test. Asterisks directly over a bar indicate a significant difference relative to WT-GFP. ($*p < 0.05$, $**p < 0.01$, $***p < 0.001$ $****p < 0.0001$).

of most cell types also accumulates other lipids, namely glycosphingolipids, which have been shown to be centrally involved in the neuropathogenesis of the disorder. Interestingly, a recent single cell transcriptome analysis of cerebella revealed that 42 % of the dysregulated genes encode sphingolipid-interacting proteins, while only 8 % of genes encoded for cholesterol binding proteins [60]. As previously mentioned, the only approved drug for NPC is miglustat [15], a molecule that inhibits the glycosphingolipids' synthesis pathway by blocking the key enzyme glucosylceramide synthase. Interestingly, enrichment of patient-derived NPC1-deficient fibroblasts with the atypical phospholipid lysobisphosphatidic acid, leads to a dramatic reduction in cholesterol accumulation in NPC1-deficient cells, stimulates autophagy, improves lysosomal function, and reduces cholesterol storage [65].

Thus, a more in-depth analysis of accumulated lipids, other than cholesterol, and the mechanisms leading to Purkinje cell death in NPC is critical to open new therapeutic avenues. Nevertheless, it is important to highlight that the onset of a visible resting tremor at 6 weeks of age suggests that increased expression of CYP46A1 earlier than 5 weeks of age could be more beneficial.

In summary, *in vivo* CYP46A1 ectopic expression ameliorates important features of NPC disease, such as cholesterol homeostasis, lysosomal function and neuroinflammation, and may represent a valid therapeutic approach to be used concomitantly with other drugs. Moreover, since our approach targets a molecular pathway that mediates neuroprotection in different models of neurodegeneration, our results may have a broaden impact on other neurodegenerative disorders with altered brain cholesterol and accelerate translation into potential therapies in areas where no significant therapeutic advances have been made.

Funding

This work was funded by FEDER and by National Funds through Fundação para a Ciência e a Tecnologia (FCT) under project PTDC/MED-NEU/29455/2017, Bolsa de Investigação da Sociedade Portuguesa de Doenças Metabólicas (SPDM), and BrainVectis Technologies.

CRediT authorship contribution statement

Maria João Nunes: Conceptualization, Formal analysis, Investigation, Methodology, Supervision, Visualization, Writing – original draft, Writing – review & editing, Project administration. **Andreia Neves Carvalho:** Investigation, Writing – review & editing. **Joana Reis:** Formal analysis, Investigation, Visualization, Writing – review & editing. **Daniela Costa:** Investigation, Writing – review & editing. **Miguel Moutinho:** Formal analysis, Investigation, Writing – review & editing. **Joana Mateus:** Investigation, Writing – review & editing. **Rita Mendes de Almeida:** Investigation, Writing – review & editing, Visualization. **Sara Brito:** Formal analysis, Investigation, Writing – review & editing. **Daniela Risso:** Investigation, Writing – review & editing. **Sofia Nunes:** Investigation, Writing – review & editing. **Margarida Castro-Caldas:** Formal analysis, Investigation, Project administration, Supervision, Writing – review & editing. **Maria João Gama:** Conceptualization, Writing – review & editing, Methodology. **Cecília M.P. Rodrigues:** Project administration, Resources, Writing – review & editing, Supervision. **Sara Xapelli:** Project administration, Resources, Writing – review & editing, Supervision. **Maria José Diógenes:** Project administration, Resources, Writing – review & editing, Supervision. **Nathalie Cartier:** Project administration, Resources, Supervision, Writing – review & editing, Conceptualization, Methodology. **Farah Chali:** Investigation, Writing – review & editing. **Françoise Piguet:** Conceptualization, Project administration, Supervision, Writing – review & editing, Methodology. **Elsa Rodrigues:** Conceptualization, Formal analysis, Funding acquisition, Project administration, Resources, Supervision, Visualization, Writing – original draft, Writing – review & editing, Methodology.

Declaration of competing interest

The authors declare the following financial interests/personal relationships which may be considered as potential competing interests:

Nathalie Cartier is a founder of BrainVectis. All other authors declare not to disclose any financial interest from the present research work.

Data availability

Data will be made available on request.

Acknowledgements

We deeply thank Doctor Lúcia Lacerda from the Centro Hospitalar Universitário do Porto EPE, Centro de Genética Médica Dr. Jacinto de Magalhães, Portugal (NPC1 $^{I1061T/I1061T}$ and NPC2 patient (NPC2^{G58T})).

Appendix A. Supplementary data

Supplementary data to this article can be found online at https://doi.org/10.1016/j.bbadis.2023.166993.

References

[1] M.T. Vanier, Niemann-pick disease type C, Orphanet J. Rare Dis. 5 (2010) 16.
[2] E.D. Carstea, J.A. Morris, K.G. Coleman, S.K. Loftus, D. Zhang, C. Cummings, J. Gu, M.A. Rosenfeld, W.J. Pavan, D.B. Krizman, J. Nagle, M.H. Polymeropoulos, S. L. Sturley, Y.A. Ioannou, M.E. Higgins, M. Comly, A. Cooney, A. Brown, C. R. Kaneski, E.J. Blanchette-Mackie, N.K. Dwyer, E.B. Neufeld, T.Y. Chang, L. Liscum, J.F. Strauss 3rd, K. Ohno, M. Zeigler, R. Carmi, J. Sokol, D. Markie, R. R. O'Neill, O.P. van Diggelen, M. Elleder, M.C. Patterson, R.O. Brady, M.T. Vanier, P.G. Pentchev, D.A. Tagle, Niemann-Pick C1 disease gene: homology to mediators of cholesterol homeostasis, Science 277 (1997) 228–231.
[3] J.P. Davies, Y.A. Ioannou, Topological analysis of Niemann-Pick C1 protein reveals that the membrane orientation of the putative sterol-sensing domain is identical to those of 3-hydroxy-3-methylglutaryl-CoA reductase and sterol regulatory element binding protein cleavage-activating protein, J. Biol. Chem. 275 (2000) 24367–24374.
[4] M.T. Vanier, Complex lipid trafficking in Niemann-pick disease type C, J. Inherit. Metab. Dis. 38 (2015) 187–199.
[5] J.E. Vance, Dysregulation of cholesterol balance in the brain: contribution to neurodegenerative diseases, Dis. Model. Mech. 5 (2012) 746–755.
[6] J.P. Liu, Y. Tang, S. Zhou, B.H. Toh, C. McLean, H. Li, Cholesterol involvement in the pathogenesis of neurodegenerative diseases, Mol Cell Neurosci, 43 33–42.

[7] Y. Higashi, S. Murayama, P.G. Pentchev, K. Suzuki, Cerebellar degeneration in the Niemann-Pick type C mouse, Acta Neuropathol. 85 (1993) 175–184.
[8] J.R. Sarna, M. Larouche, H. Marzban, R.V. Sillitoe, D.E. Rancourt, R. Hawkes, Patterned Purkinje cell degeneration in mouse models of Niemann-pick type C disease, J. Comp. Neurol. 456 (2003) 279–291.
[9] J.E. Vance, B. Karten, Niemann-pick C disease and mobilization of lysosomal cholesterol by cyclodextrin, J. Lipid Res. 55 (2014) 1609–1621.
[10] P.C. Reid, N. Sakashita, S. Sugii, Y. Ohno-Iwashita, Y. Shimada, W.F. Hickey, T. Y. Chang, A novel cholesterol stain reveals early neuronal cholesterol accumulation in the Niemann-pick type C1 mouse brain, J. Lipid Res. 45 (2004) 582–591.
[11] L. Kavetsky, K.K. Green, B.R. Boyle, F.A.K. Yousufzai, Z.M. Padron, S.E. Melli, V. L. Kuhnel, H.M. Jackson, R.E. Blanco, G.R. Howell, I. Soto, Increased interactions and engulfment of dendrites by microglia precede Purkinje cell degeneration in a mouse model of Niemann pick type-C, Sci. Rep. 9 (2019) 14722.
[12] A. Cougnoux, S. Clifford, A. Salman, S.L. Ng, J. Bertin, F.D. Porter, Necroptosis inhibition as a therapy for Niemann-pick disease, type C1: inhibition of RIP kinases and combination therapy with 2-hydroxypropyl-beta-cyclodextrin, Mol. Genet. Metab. 125 (2018) 345–350.
[13] E. Lloyd-Evans, A.J. Morgan, X. He, D.A. Smith, E. Elliot-Smith, D.J. Sillence, G. C. Churchill, E.H. Schuchman, A. Galione, F.M. Platt, Niemann-pick disease type C1 is a sphingosine storage disease that causes deregulation of lysosomal calcium, Nat. Med. 14 (2008) 1247–1255.
[14] W. Yu, J.S. Gong, M. Ko, W.S. Garver, K. Yanagisawa, M. Michikawa, Altered cholesterol metabolism in Niemann-pick type C1 mouse brains affects mitochondrial function, J. Biol. Chem. 280 (2005) 11731–11739.
[15] D. Sitarska, A. Tylki-Szymanska, A. Lugowska, Treatment trials in Niemann-pick type C disease, Metab. Brain Dis. 36 (2021) 2215–2221.
[16] I. Bjorkhem, D. Lutjohann, U. Diczfalusy, L. Stahle, G. Ahlborg, J. Wahren, Cholesterol homeostasis in human brain: turnover of 24S-hydroxycholesterol and evidence for a cerebral origin of most of this oxysterol in the circulation, J. Lipid Res. 39 (1998) 1594–1600.
[17] E.G. Lund, J.M. Guileyardo, D.W. Russell, cDNA cloning of cholesterol 24-hydroxylase, a mediator of cholesterol homeostasis in the brain, Proc. Natl. Acad. Sci. U. S. A. 96 (1999) 7238–7243.
[18] E.G. Lund, C. Xie, T. Kotti, S.D. Turley, J.M. Dietschy, D.W. Russell, Knockout of the cholesterol 24-hydroxylase gene in mice reveals a brain-specific mechanism of cholesterol turnover, J. Biol. Chem. 278 (2003) 22980–22988.
[19] S. Maioli, A. Bavner, Z. Ali, M. Heverin, M.A. Ismail, E. Puerta, M. Olin, A. Saeed, M. Shafaati, P. Parini, A. Cedazo-Minguez, I. Bjorkhem, Is it possible to improve memory function by upregulation of the cholesterol 24S-hydroxylase (CYP46A1) in the brain? PloS One 8 (2013) e68534.
[20] T. Kotti, D.D. Head, C.E. McKenna, D.W. Russell, Biphasic requirement for geranylgeraniol in hippocampal long-term potentiation, Proc. Natl. Acad. Sci. U. S. A. 105 (2008) 11394–11399.
[21] T.J. Kotti, D.M. Ramirez, B.E. Pfeiffer, K.M. Huber, D.W. Russell, Brain cholesterol turnover required for geranylgeraniol production and learning in mice, Proc. Natl. Acad. Sci. U. S. A. 103 (2006) 3869–3874.
[22] M. Moutinho, M.J. Nunes, A.Q. Gomes, M.J. Gama, A. Cedazo-Minguez, C. M. Rodrigues, I. Bjorkhem, E. Rodrigues, Cholesterol 24S-hydroxylase overexpression inhibits the liver X receptor (LXR) pathway by activating small guanosine triphosphate-binding proteins (sGTPases) in neuronal cells, Mol. Neurobiol. 51 (2015) 1489–1503.
[23] M. Moutinho, M.J. Nunes, J.C. Correia, M.J. Gama, M. Castro-Caldas, A. Cedazo-Minguez, C.M. Rodrigues, I. Bjorkhem, J.L. Ruas, E. Rodrigues, Neuronal cholesterol metabolism increases dendritic outgrowth and synaptic markers via a concerted action of GGTase-I and Trk, Sci. Rep. 6 (2016) 30928.
[24] M.A. Burlot, J. Braudeau, K. Michaelsen-Preusse, B. Potier, S. Ayciriex, J. Varin, B. Gautier, F. Djelti, M. Audrain, L. Dauphinot, F.J. Fernandez-Gomez, R. Caillierez, O. Laprevote, I. Bieche, N. Auzeil, M.C. Potier, P. Dutar, M. Korte, L. Buee, D. Blum, N. Cartier, Cholesterol 24-hydroxylase defect is implicated in memory impairments associated with Alzheimer-like tau pathology, Hum. Mol. Genet. 24 (2015) 5965–5976.
[25] E. Hudry, D. Van Dam, W. Kulik, P.P. De Deyn, F.S. Stet, O. Ahouansou, A. Benraiss, A. Delacourte, P. Bougneres, P. Aubourg, N. Cartier, Adeno-associated virus gene therapy with cholesterol 24-hydroxylase reduces the amyloid pathology before or after the onset of amyloid plaques in mouse models of Alzheimer's disease, Molecular Therapy: The Journal of the American Society of Gene Therapy 18 (2010) 44–53.
[26] L. Boussicault, S. Alves, A. Lamaziere, A. Planques, N. Heck, L. Moumne, G. Despres, S. Bolte, A. Hu, C. Pages, L. Galvan, F. Piguet, P. Aubourg, N. Cartier, J. Caboche, S. Betuing, CYP46A1, the rate-limiting enzyme for cholesterol degradation, is neuroprotective in Huntington's disease, Brain J. Neurol. 139 (2016) 953–970.
[27] C. Nobrega, L. Mendonca, A. Marcelo, A. Lamaziere, S. Tome, G. Despres, C. A. Matos, F. Mechmet, D. Langui, W. den Dunnen, L.P. de Almeida, N. Cartier, S. Alves, Restoring brain cholesterol turnover improves autophagy and has therapeutic potential in mouse models of spinocerebellar ataxia, Acta Neuropathol. 138 (2019) 837–858.
[28] E. Audouard, V. Oger, B. Meha, N. Cartier, C. Sevin, F. Piguet, Complete correction of brain and spinal cord pathology in metachromatic Leukodystrophy mice, Front. Mol. Neurosci. 14 (2021) 677895.
[29] S.N. Mathiesen, J.L. Lock, L. Schoderboeck, W.C. Abraham, S.M. Hughes, CNS transduction benefits of AAV-PHP.eB over AAV9 are dependent on administration route and mouse strain, Mol Ther Methods Clin Dev 19 (2020) 447–458.
[30] M. Praggastis, B. Tortelli, J. Zhang, H. Fujiwara, R. Sidhu, A. Chacko, Z. Chen, C. Chung, A.P. Lieberman, J. Sikora, C. Davidson, S.U. Walkley, N.H. Pipalia, F. R. Maxfield, J.E. Schaffer, D.S. Ory, A murine Niemann-pick C1 I1061T knock-in model recapitulates the pathological features of the most prevalent human disease allele, the journal of neuroscience: the official journal of the society for, Neuroscience 35 (2015) 8091–8106.
[31] S. Moreira, I. Fonseca, M.J. Nunes, A. Rosa, L. Lemos, E. Rodrigues, A.N. Carvalho, T.F. Outeiro, C.M.P. Rodrigues, M.J. Gama, M. Castro-Caldas, Nrf2 activation by tauroursodeoxycholic acid in experimental models of Parkinson's disease, Exp. Neurol. 295 (2017) 77–87.
[32] C.L. Andersen, J.L. Jensen, T.F. Orntoft, Normalization of real-time quantitative reverse transcription-PCR data: a model-based variance estimation approach to identify genes suited for normalization, applied to bladder and colon cancer data sets, Cancer Res. 64 (2004) 5245–5250.
[33] F.M. Mouro, V.L. Batalha, D.G. Ferreira, J.E. Coelho, Y. Baqi, C.E. Muller, L. V. Lopes, J.A. Ribeiro, A.M. Sebastiao, Chronic and acute adenosine a(2A) receptor blockade prevents long-term episodic memory disruption caused by acute cannabinoid CB(1) receptor activation, Neuropharmacology 117 (2017) 316–327.
[34] F.R. Maxfield, D. Wustner, Analysis of cholesterol trafficking with fluorescent probes, Methods Cell Biol. 108 (2012) 367–393.
[35] R.P. Erickson, A. Bhattacharyya, R.J. Hunter, R.A. Heidenreich, N.J. Cherrington, Liver disease with altered bile acid transport in Niemann-pick C mice on a high-fat, 1% cholesterol diet, Am. J. Physiol. Gastrointest. Liver Physiol. 289 (2005) G300–G307.
[36] H. Li, J.J. Repa, M.A. Valasek, E.P. Beltroy, S.D. Turley, D.C. German, J. M. Dietschy, Molecular, anatomical, and biochemical events associated with neurodegeneration in mice with Niemann-pick type C disease, J. Neuropathol. Exp. Neurol. 64 (2005) 323–333.
[37] E. Santiago-Mujica, S. Flunkert, R. Rabl, J. Neddens, T. Loeffler, B. Hutter-Paier, Hepatic and neuronal phenotype of NPC1(−/−) mice, Heliyon 5 (2019) e01293.
[38] C. Xie, S.D. Turley, P.G. Pentchev, J.M. Dietschy, Cholesterol balance and metabolism in mice with loss of function of Niemann-Pick C protein, Am. J. Physiol. 276 (1999) E336–E344.
[39] V. Hirsch-Reinshagen, S. Zhou, B.L. Burgess, L. Bernier, S.A. McIsaac, J.Y. Chan, G. H. Tansley, J.S. Cohn, M.R. Hayden, C.L. Wellington, Deficiency of ABCA1 impairs apolipoprotein E metabolism in brain, J. Biol. Chem. 279 (2004) 41197–41207.
[40] G. Liao, Y. Yao, J. Liu, Z. Yu, S. Cheung, A. Xie, X. Liang, X. Bi, Cholesterol accumulation is associated with lysosomal dysfunction and autophagic stress in Npc1 −/− mouse brain, Am. J. Pathol. 171 (2007) 962–975.
[41] A. Cougnoux, R.A. Drummond, A.L. Collar, J.R. Iben, A. Salman, H. Westgarth, C. A. Wassif, N.X. Cawley, N.Y. Farhat, K. Ozato, M.S. Lionakis, F.D. Porter, Microglia activation in Niemann-pick disease, type C1 is amendable to therapeutic intervention, Hum. Mol. Genet. 27 (2018) 2076–2089.
[42] S.R. Subramaniam, H.J. Federoff, Targeting microglial activation states as a therapeutic avenue in Parkinson's disease, Front. Aging Neurosci. 9 (2017) 176.
[43] D.S.A. Simpson, P.L. Oliver, ROS generation in Microglia: understanding oxidative stress and inflammation in neurodegenerative disease, Antioxidants (Basel) 9 (2020).
[44] Z. Ahmed, G. Shaw, V.P. Sharma, C. Yang, E. McGowan, D.W. Dickson, Actin-binding proteins coronin-1a and IBA-1 are effective microglial markers for immunohistochemistry, J. Histochem. Cytochem. 55 (2007) 687–700.
[45] S.M. Cologna, C.V. Cluzeau, N.M. Yanjanin, P.S. Blank, M.K. Dail, S. Siebel, C. L. Toth, C.A. Wassif, A.P. Lieberman, F.D. Porter, Human and mouse neuroinflammation markers in Niemann-Pick disease, type C1, J. Inherit. Metab. Dis. 37 (2014) 83–92.
[46] P. Caporali, F. Bruno, G. Palladino, J. Dragotto, L. Petrosini, F. Mangia, R. P. Erickson, S. Canterini, M.T. Fiorenza, Developmental delay in motor skill acquisition in Niemann-pick C1 mice reveals abnormal cerebellar morphogenesis, Acta Neuropathol. Commun. 4 (2016) 94.
[47] A. Buffo, F. Rossi, Origin, lineage and function of cerebellar glia, Prog. Neurobiol. 109 (2013) 42–63.
[48] M. Laure-Kamionowska, D. Maslinska, Calbindin positive Purkinje cells in the pathology of human cerebellum occurring at the time of its development, Folia Neuropathol. 47 (2009) 300–305.
[49] M. Gomez-Grau, J. Albaiges, J. Casas, C. Auladell, M. Dierssen, L. Vilageliu, D. Grinberg, New murine Niemann-pick type C models bearing a pseudoexon-generating mutation recapitulate the main neurobehavioural and molecular features of the disease, Sci. Rep. 7 (2017) 41931.
[50] Y.H. Hung, M. Walterfang, L. Churilov, L. Bray, L.H. Jacobson, K.J. Barnham, N. C. Jones, T.J. O'Brien, D. Velakoulis, A.I. Bush, Neurological dysfunction in early maturity of a model for Niemann-Pick C1 carrier status, Neurotherapeutics 13 (2016) 614–622.
[51] J. Davidson, E. Molitor, S. Moores, S.E. Gale, K. Subramanian, X. Jiang, R. Sidhu, P. Kell, J. Zhang, H. Fujiwara, C. Davidson, P. Helquist, B.J. Melancon, M. Grigalunas, G. Liu, F. Salahi, O. Wiest, X. Xu, F.D. Porter, N.H. Pipalia, D. L. Cruz, E.B. Holson, J.E. Schaffer, S.U. Walkley, F.R. Maxfield, D.S. Ory, 2-Hydroxypropyl-beta-cyclodextrin is the active component in a triple combination formulation for treatment of Niemann-Pick C1 disease, Biochim. Biophys. Acta Mol. Cell Biol. Lipids 2019 (1864) 1545–1561.
[52] E. Boadu, R.C. Nelson, G.A. Francis, ABCA1-dependent mobilization of lysosomal cholesterol requires functional Niemann-Pick C2 but not Niemann-Pick C1 protein, Biochim. Biophys. Acta 1821 (2012) 396–404.
[53] F.X. Guix, A.M. Capitan, A. Casadome-Perales, I. Palomares-Perez, I. Lopez Del Castillo, V. Miguel, L. Goedeke, M.G. Martin, S. Lamas, H. Peinado, C. Fernandez-Hernando, C.G. Dotti, Increased exosome secretion in neurons aging in vitro by NPC1-mediated endosomal cholesterol buildup, Life Sci Alliance 4 (2021).
[54] O.B. Davis, H.R. Shin, C.Y. Lim, E.Y. Wu, M. Kukurugya, C.F. Maher, R.M. Perera, M.P. Ordonez, R. Zoncu, NPC1-mTORC1 signaling couples cholesterol sensing to

organelle homeostasis and is a targetable pathway in Niemann-Pick type C, Dev. Cell 56 (2021) 260–276 e267.
[55] S. Sarkar, B. Carroll, Y. Buganim, D. Maetzel, A.H. Ng, J.P. Cassady, M.A. Cohen, S. Chakraborty, H. Wang, E. Spooner, H. Ploegh, J. Gsponer, V.I. Korolchuk, R. Jaenisch, Impaired autophagy in the lipid-storage disorder Niemann-Pick type C1 disease, Cell Rep. 5 (2013) 1302–1315.
[56] K. Frudd, T. Burgoyne, J.R. Burgoyne, Oxidation of Atg3 and Atg7 mediates inhibition of autophagy, Nat. Commun. 9 (2018) 95.
[57] Y.K. Seo, T.I. Jeon, H.K. Chong, J. Biesinger, X. Xie, T.F. Osborne, Genome-wide localization of SREBP-2 in hepatic chromatin predicts a role in autophagy, Cell Metab. 13 (2011) 367–375.
[58] A. Cougnoux, J.C. Yerger, M. Fellmeth, J. Serra-Vinardell, K. Martin, F. Navid, J. Iben, C.A. Wassif, N.X. Cawley, F.D. Porter, Single cell transcriptome analysis of Niemann-pick disease, type C1 cerebella, Int. J. Mol. Sci. 21 (2020).
[59] M.S. Thion, D. Low, A. Silvin, J. Chen, P. Grisel, J. Schulte-Schrepping, R. Blecher, T. Ulas, P. Squarzoni, G. Hoeffel, F. Coulpier, E. Siopi, F.S. David, C. Scholz, F. Shihui, J. Lum, A.A. Amoyo, A. Larbi, M. Poidinger, A. Buttgereit, P.M. Lledo, M. Greter, J.K.Y. Chan, I. Amit, M. Beyer, J.L. Schultze, A. Schlitzer, S. Pettersson, F. Ginhoux, S. Garel, Microbiome Influences Prenatal, Adult Microglia, A sex-specific manner, Cell 172 (2018) 500–516, e516.
[60] M. Zhang, D. Strnatka, C. Donohue, J.L. Hallows, I. Vincent, R.P. Erickson, Astrocyte-only Npc1 reduces neuronal cholesterol and triples life span of Npc1−/− mice, J. Neurosci. Res. 86 (2008) 2848–2856.
[61] D.N. Mitroi, G. Pereyra-Gomez, B. Soto-Huelin, F. Senovilla, T. Kobayashi, J. A. Esteban, M.D. Ledesma, NPC1 enables cholesterol mobilization during long-term potentiation that can be restored in Niemann-pick disease type C by CYP46A1 activation, EMBO Rep. 20 (2019) e48143.
[62] R.A. Maue, R.W. Burgess, B. Wang, C.M. Wooley, K.L. Seburn, M.T. Vanier, M. A. Rogers, C.C. Chang, T.Y. Chang, B.T. Harris, D.J. Graber, C.A. Penatti, D. M. Porter, B.S. Szwergold, L.P. Henderson, J.W. Totenhagen, T.P. Trouard, I. A. Borbon, R.P. Erickson, A novel mouse model of Niemann-Pick type C disease carrying a D1005G-Npc1 mutation comparable to commonly observed human mutations, Hum. Mol. Genet. 21 (2012) 730–750.
[63] N. Mast, A. Saadane, A. Valencia-Olvera, J. Constans, E. Maxfield, H. Arakawa, Y. Li, G. Landreth, I.A. Pikuleva, Cholesterol-metabolizing enzyme cytochrome P450 46A1 as a pharmacologic target for Alzheimer's disease, Neuropharmacology 123 (2017) 465–476.
[64] N. Mast, N. El-Darzi, A.M. Petrov, Y. Li, I.A. Pikuleva, CYP46A1-dependent and independent effects of efavirenz treatment, Brain Commun 2 (2020) fcaa180.
[65] O. Ilnytska, K. Lai, K. Gorshkov, M.L. Schultz, B.N. Tran, M. Jeziorek, T.J. Kunkel, R.D. Azaria, H.S. McLoughlin, M. Waghalter, Y. Xu, M. Schlame, N. Altan-Bonnet, W. Zheng, A.P. Lieberman, R. Dobrowolski, J. Storch, Enrichment of NPC1-deficient cells with the lipid LBPA stimulates autophagy, improves lysosomal function, and reduces cholesterol storage, J. Biol. Chem. 297 (2021) 100813.